Chaos, Solitons and Fractals 172 (2023) 113560

Contents lists available at ScienceDirect

Chaos, Solitons and Fractals

journal homepage: www.elsevier.com/locate/chaos

A statistical moment-based spectral approach to the chance-constrained stochastic optimal control of epidemic models

Alberto Olivares[1], Ernesto Staffetti[1,*]

Universidad Rey Juan Carlos, Camino del Molino 5, 28942 Fuenlabrada, Madrid, Spain

ARTICLE INFO

Keywords:
Arbitrary polynomial chaos
Stochastic optimal control
Chance constraints
Epidemic models
COVID-19

ABSTRACT

This paper presents a spectral approach to the uncertainty management in epidemic models through the formulation of chance-constrained stochastic optimal control problems. Specifically, a statistical moment-based polynomial expansion is used to calculate surrogate models of the stochastic state variables of the problem that allow for the efficient computation of their main statistics as well as their marginal and joint probability density functions at each time instant, which enable the uncertainty management in the epidemic model. Moreover, the surrogate models are employed to perform the corresponding sensitivity and risk analyses. The proposed methodology provides the designers of the optimal control policies with the capability to increase the predictability of the outcomes by adding suitable chance constraints to the epidemic model and formulating a proper cost functional. The chance-constrained optimal control of a COVID-19 epidemic model is considered in order to illustrate the practical application of the proposed methodology.

1. Introduction

The spectral approach to uncertainty propagation and quantification in model-based systems is a powerful methodology that can be employed for sensitivity analysis, uncertainty management, and risk analysis [1].

The sensitivity analysis, usually based on the variance of the model output, provides a useful decision support tool for system design and optimization. It quantifies the variation of the system response around a nominal value and allows for the characterization of the robustness of the predictions as well as the controllability of the system. Moreover, when the system is subject to multiple sources of uncertainty, the sensitivity analysis can be used to quantify their relative influence on the system response. This information is crucial in the determination of uncertainty management strategies with the aim of reducing the main sources of uncertainty. Furthermore, it is often useful to assess the probabilities of a system output variable exceeding specific critical thresholds using the statistical properties of the random input data. These probabilities can then be employed to undertake system reliability or risk analyses.

This paper focuses on the optimal control approach to the uncertainty management in epidemic models. More specifically, epidemic disease transmission is assumed to be represented by means of compartmental models, in which the population is subdivided into compartments and several assumptions are made about the nature and time rate of transition between them. Compartmental epidemic models are one of the main approaches to the mathematical modelling of epidemic disease transmission, which have been used to analyse the specific behaviour of various infections [2,3].

The mitigation and control of the spread of an epidemic disease have the features of an Optimal Control Problem (OCP). More specifically, the goal is to minimize some objective functional usually associated with the number of infected subjects or the cost of the control strategies against the disease transmission, which can be related to both non-pharmacological and pharmacological measures. Furthermore, the disease transmission and its interactions with the control policies are described by the underlying dynamical system and the algebraic constraints imposed.

The solutions of an OCP may be affected by the presence of external disturbances and model uncertainties, which are not easy to incorporate into a deterministic mathematical representation of the system. In these cases, a Stochastic OCP (SOCP) must be formulated, in which a set of stochastic differential equations describes the dynamical system. In particular, in this paper, the stochastic epidemic models are assumed to be represented by sets of nonlinear Ordinary Differential Equations (ODEs) with random parameters [4], namely some of the parameters of the ODE system are supposed to be the source of uncertainty of the SOCP. Hence, systems of stochastic Itô-type differential equations [5] and Markovian differential equations [6], as

* Corresponding author.
E-mail addresses: alberto.olivares@urjc.es (A. Olivares), ernesto.staffetti@urjc.es (E. Staffetti).
[1] All authors contributed equally to this work.

https://doi.org/10.1016/j.chaos.2023.113560
Received 16 November 2022; Received in revised form 2 May 2023; Accepted 9 May 2023
Available online 24 May 2023

well as systems of stochastic partial differential equations [7], are not considered in this paper.

The deterministic optimal control approach has been extensively applied to the control of epidemic diseases. For the sake of brevity, only the following recent publications are featured. Different optimal control strategies of a fractional order model for Zika virus infection are presented in [8]. A dynamic model of the dengue strain is used in [9] to formulate an OCP, in which the number of people infected is minimized by applying mosquito removal measures. The optimal control of a HIV/AIDS-resistant model with behaviour change is proposed in [10], which considers as controls the government's intervention in encouraging behaviour change, the intake of balanced nutritional supplementation, and the antiretroviral therapy. The effectiveness of antidotes and vaccination in restraining viral creation and decelerating the production of new influenza infections is studied in [11], in which a structured model based on urban and rural areas is considered. A Zika control model is developed and optimized in [12], which incorporates three different control measures, namely prevention through bed nets and mosquito repellents, patients' treatment, and insecticides. An OCP is formulated in [13], employing a mathematical model of dengue transmission, to quantify the impact of information-based behavioural response and the segregation of the infected human population into detected and undetected individuals. In [14], an optimal control approach is used to analyse the transmission dynamics of HIV/AIDS by combining two control measures, namely standard antiretroviral therapy and AIDS treatments. The optimal allocation of vaccine and antiviral drugs for influenza containment over a time-delayed two-stage epidemic model is studied in [15]. The optimal control problem of a fractional-order delayed epidemic model with a saturated incidence rate and saturated treatment function is studied in [16], in which vaccination and increasing treatment intensity are the control interventions.

Less research effort has been devoted to the stochastic optimal control of epidemic diseases. The most recent articles on this topic are surveyed. The optimal control of a stochastic mathematical model with random transmission for the hepatitis B virus is studied in [17]. A state estimation-based robust optimal control strategy for influenza epidemics in an interactive human society is presented in [18]. The optimal control of the spread of the hepatitis B virus through the strategy of vaccinating offspring is proposed in [19], which is based on a stochastic model with random noise transmission. The optimal control of a stochastic dengue model described by spatial diffusion and Brownian motion is proposed in [20]. The robust optimal control of a network-based epidemic system with an uncertain time delay is investigated in [21], in which time-dependent and degree-dependent vaccination controls are considered. The optimal vaccination strategy for an hepatitis B epidemic model with the inclusion of white noise and Markovian switching is analysed in [22]. Several OCPs for various epidemic models with uncertainty are formulated in [23], which are solved using deep reinforcement learning. A robust economic model predictive controller for the management of stochastic epidemic processes is developed in [24], which efficiently drives the epidemic process to extinction while minimizing the use of control resources.

Optimal control-based works focused on the mitigation and control of the COVID-19 pandemic deserve a special mention. Both deterministic and stochastic approaches have been proposed. The most relevant articles on this topic are surveyed.

A model predictive approach for the constrained control of a nonlinear compartmental model that captures the key dynamical properties of COVID-19 is considered in [25], which is able to handle complex, time-dependent constraints, logical relations between model variables, and multiple predefined discrete levels of interventions. A nonlinear Model Predictive Control (MPC) method for the mitigation of the COVID-19 outbreak in a multi-region scenario is proposed in [26], which minimizes the cost of non-pharmaceutical interventions. A nonlinear MPC approach to optimally schedule the first and second vaccination doses is presented in [27], which takes into account both healthcare needs and socio-economic costs associated with the COVID-19 pandemic. The suppression of the spread of COVID-19 by means of rapid test intervention is analysed in [28]. The impact of isolation, vaccine efficacy, and treatment enhancement in controlling the COVID-19 outbreak is evaluated in [29].

A chance-constrained optimal control model of the COVID-19 pandemic spread is proposed in [30], in which the effects of isolation and weather are investigated. Robust optimal nonpharmaceutical strategies, based on a stochastic nonlinear model predictive controller, are proposed in [31] to tackle the COVID-19 pandemic waves. The optimal quarantine control of a stochastic reaction–diffusion epidemic model for the COVID-19 infectious disease is presented in [32]. The minimum average quarantine duration for uninfected people is determined in [33], in which the constraint that the probability of symptom presentation for COVID-19 infected people attains a given value is imposed. A probabilistic MPC approach is proposed in [34], which allows social distancing policies for the COVID-19 pandemic to be designed. The optimal allocation of stockpiles of COVID-19 vaccines and tests to a set of zones is presented in [35], in which different sources of uncertainty are considered.

There are different approaches to the formulation and resolution of Chance-Constrained Stochastic OCP (CCSOCP), such as Polynomial Chaos Expansion (PCE) and subset simulation [36], kernel density estimation [37], Hilbert space embedding [38], and second-order cone programming [39]. In particular, this paper follows a data-driven PCE approach to the chance-constrained optimal control of epidemic models. PCE is a spectral methodology for the uncertainty quantification of computational models, which was introduced in [40], generalized in [41], and further extended to arbitrary distributions in [42]. Given a computational model, the PCE technique allows the model outputs to be projected on a basis of orthogonal stochastic polynomials in the random inputs, which provides an efficient representation of the outputs' variability in terms of the variability of the inputs. The PCE approach has been successfully applied to a wide variety of research areas, including the stability and control of both deterministic and stochastic systems [43,44].

This paper presents a spectral approach to the uncertainty management in epidemic models through the formulation of CCSOCPs, which also allows the corresponding sensitivity and risk analyses to be performed. More specifically, a statistical moment-based polynomial expansion is used to calculate surrogate models of the stochastic state variables of the problem, which enables the efficient computation of their main statistics as well as their marginal and joint Probability Density Functions (PDFs) at each time instant. These surrogate models are used to reformulate the CCSOCPs as augmented deterministic optimal control problems. Moreover, they are also employed to conduct a global sensitivity analysis in terms of the so-called Sobol' indices, as well as a risk analysis based on Monte Carlo (MC) simulations and kernel density estimations of the marginal and joint PDFs of the optimal stochastic state variables. To the best knowledge of the authors, the spectral approach to the uncertainty management in epidemic models through chance-constrained optimal control has not been addressed yet in the literature.

The paper is organized as follows. Section 2 presents the general formulation of the CCSOCP, which is based on the definition of a SOCP. The two main approaches to the formulation of a robust constrained SOCP are described in Section 3. Section 4 introduces the statistical moment-based spectral approach to the uncertainty propagation and quantification in the CCSOCP. Section 5 outlines the computational and statistical properties of the surrogate models of the state variables represented by their aPC expansions, which allow the uncertainty management to be performed as well as the sensitivity and risk analyses. In Section 6, the reformulation of the CCSOCP as an augmented deterministic OCP is presented. The practical implementation of the proposed spectral approach is shown in Section 7, in which the chance-constrained stochastic optimal control of a COVID-19 epidemic model is described. The results of several numerical experiments are reported and discussed in Section 8. Finally, some conclusions are drawn in Section 9.

2. Chance-constrained stochastic optimal control

This section presents the general formulation of the CCSOCP considered in this paper, which is based on the definition of a SOCP.

Optimal control is a research discipline that deals with finding the controls that guide a dynamical system from an initial to a final state while optimizing an objective functional. Controls are represented as functions of time that characterize allowable external influences on a system and cause a system response. Based on this response, the objective functional is assessed and used as a measure of the system's performance.

As mentioned in Section 1, the presence of external disturbances and model uncertainties leads to the formulation of SOCPs. The solutions of a SOCP are required to be robust, namely the control system specifications must be fulfilled independently of the realization of the random parameters. The robustness of the solutions implies the inclusion of statistical moments or probabilities of events in the constraints and in the objective functional of the SOCP. SOCPs in which the constraints are expressed in terms of statistical moments are usually known as Robust Constrained SOCPs (RCSOCPs), whereas they are referred to as CCSOCPs when the constraints are represented as probabilities of events.

2.1. Statement of the stochastic optimal control problem

Let $(\Omega, \Lambda, \Gamma)$ be a probability space, where Ω is the space of events, Λ is a σ-algebra, and Γ is a probability measure. Then, the SOCP considered in this paper can be stated as follows:

$$\min_{\mathbf{u}(t)} \quad \mathcal{J}(\mathbf{x}(t,\xi),\mathbf{u}(t),\xi) = \mathcal{M}(\mathbf{x}(t_F,\xi)) + \int_{t_I}^{t_F} \mathcal{L}(\mathbf{x}(t,\xi),\mathbf{u}(t),\xi)\, dt, \tag{1a}$$

subject to:

$$\dot{\mathbf{x}}(t,\xi) = \mathbf{f}(\mathbf{x}(t,\xi),\mathbf{u}(t),\xi) \quad \text{a.s.}, \tag{1b}$$

$$\mathbf{x}(t_I,\xi) = \mathbf{x}_I, \quad \mathbf{x}(t_F,\xi) = \mathbf{x}_F \quad \text{a.s.}, \tag{1c}$$

where t denotes time, $\mathbf{x}(t,\xi) = (x_1(t,\xi),\dots,x_n(t,\xi))$ is the vector of stochastic state variables, $\mathbf{u}(t) = (u_1(t),\dots,u_m(t))$ is the vector of control variables, and $\xi = (\xi_1,\dots,\xi_{N_U}) \in \Omega$ is the vector of random parameters, which describes the uncertainties of the SOCP. The components of the vector of random parameters ξ are assumed to be independent random variables. Therefore, the joint PDF of ξ can be obtained as $g(\xi) = \prod_{i=1}^{N_U} g_i(\xi_i)$, with $g_i(\xi_i)$ being the marginal PDF of each random variable ξ_i, $i = 1,\dots,N_U$. The initial and final time instants are denoted by t_I and t_F, respectively, whereas $\mathbf{x}_I$ and $\mathbf{x}_F$ are the vectors of initial and final states, respectively.

In (1a), the objective functional $\mathcal{J}(\cdot)$, which represents the cost index related to the control strategies against the disease transmission, is given in Bolza form, namely it is formulated as a combination of the Mayer term $\mathcal{M}(\cdot)$ and the Lagrange term $\mathcal{L}(\cdot)$. The Mayer term represents a terminal cost, whereas the Lagrange term represents a running cost. Notice that, without loss of generality, the objective functional (1a) can be expressed in Mayer form, since the Lagrange term can be reformulated as a Mayer term by introducing a new state variable and adding a new differential equation [45].

Eqs. (1b) and (1c), respectively, corresponds to the set of differential equations and the boundary conditions that represent the dynamical equations and the initial and final conditions of the stochastic epidemic model.

Notice that, in (1), the objective functional and the differential equations are stochastic functions. Moreover, the state variables $\mathbf{x}(t,\xi)$ are functions of both the time t and the vector of random parameters ξ, and the stochastic relations are assumed to be satisfied almost surely (a.s.). Conversely, the control variables $\mathbf{u}(t)$ are assumed to be deterministic functions of time t.

2.2. Statement of the chance-constrained stochastic optimal control problem

The CCSOCP considered in this work can be stated as follows:

$$\min_{\mathbf{u}(t)} \quad \mu\left(\mathcal{J}(\mathbf{x}(t,\xi),\mathbf{u}(t),\xi)\right) + \kappa_0 \cdot \sigma\left(\mathcal{J}(\mathbf{x}(t,\xi),\mathbf{u}(t),\xi)\right), \tag{2a}$$

subject to:

$$\dot{\mathbf{x}}(t,\xi) = \mathbf{f}(\mathbf{x}(t,\xi),\mathbf{u}(t),\xi) \quad \text{a.s.}, \tag{2b}$$

$$P\left(\mathbf{a}\ \mathbf{x}(t,\xi) \le \mathbf{b}\right) \ge \mathbf{1} - \boldsymbol{\eta}, \tag{2c}$$

$$\mu\left(\mathbf{x}(t_I,\xi)\right) = \mathbf{x}_I, \sigma\left(\mathbf{x}(t_I,\xi)\right) \le \varepsilon_I,$$

$$\mu\left(\mathbf{x}(t_F,\xi)\right) = \mathbf{x}_F, \sigma\left(\mathbf{x}(t_F,\xi)\right) \le \varepsilon_F, \tag{2d}$$

where κ_0, ε_I, and ε_F are parameters, $\mathbf{a} = (a_1,\dots,a_{n_C})$, $\mathbf{b} = (b_1,\dots,b_{n_C})$, and $\boldsymbol{\eta} = (\eta_1,\dots,\eta_{n_C})$, with $1 \le n_C \le n$, are parameter vectors, $P(\cdot)$, $\mu(\cdot)$, and $\sigma(\cdot)$ denote the probability, the expected value, and the standard deviation operators, respectively, and the remaining variables and functions are defined as in (1).

In the statement of the CCSOCP (2), the inequality (2c) corresponds to a chance constraint on the vector of stochastic state variables, in which $\mathbf{1} - \boldsymbol{\eta} = (1-\eta_1,\dots,1-\eta_{n_C})$, where the value $1-\eta_l, l = 1,\dots,n_C$, is known as guaranteed constraint satisfaction probability or chance constraint probability, and the parameter $\eta_l, l = 1,\dots,n_C$, is referred to as probability of violation or risk level. The chance constraint (2c) allows stochastic algebraic constraints to be included in the formulation of the SOCP (1), which permits the uncertainty management in the optimal control of the stochastic epidemic model represented by Eqs. (1b) and (1c) to be conducted.

Notice that, for the sake of ease of notation, the formulation of the CCSOCP (2) is understood element-wise. Thus, the chance constraint (2c) actually denotes

$$P\left(a_1\ x_1(t,\xi) \le b_1\right) \le 1-\eta_1,\dots,P\left(a_{n_C}\ x_{n_C}(t,\xi) \le b_{n_C}\right) \le 1-\eta_{n_C}, \tag{3}$$

with $1 \le n_C \le n$, namely a chance constraint is imposed on at least one out of the n components of the vector of stochastic state variables $\mathbf{x}(t,\xi)$. Each chance constraint $P\left(a_l\ x_l(t,\xi) \le b_l\right) \le 1-\eta_l$, $l = 1,\dots,n_C$, here is referred to as single chance constraint.

Moreover, in the statement of the CCSOCP (2), a robust formulation of the objective functional and the boundary values is considered. Specifically, the robust formulation of the objective functional (2a) consists of a weighted sum of the expected value and the standard deviation of the stochastic objective functional (1a), where κ_0 denotes the weighting parameter. Conversely, the robustness of the boundary values (2d) is modelled by splitting the expected value and the standard deviation of (1c). The expected values of the boundary conditions are forced to satisfy the same requirements stated in (1c), whereas the values of the standard deviation of these boundary conditions are forced to satisfy specific upper bounds denoted by ε_I and ε_F.

Notice that the weight κ_0, the probabilities $\eta_l, l = 1,\dots,n_C$, and the upper bounds ε_I and ε_F must be set by the designers of the CCSOCP.

2.3. Joint chance constraints

Suppose that, in the formulation of the CCSOCP (2), instead of the inequality constraint (2c), which is composed of a set of single chance constraints, the following constraint is considered:

$$P\left(a_1\ x_1(t,\xi) \le b_1,\dots,a_{n_C}\ x_{n_C}(t,\xi) \le b_{n_C}\right) \ge 1-\eta, \quad \text{with} \quad 1 \le n_C \le n, \tag{4}$$

which will be referred to as joint chance constraint. Then, using Bonferroni's inequality [46], the joint chance constraint (4) can be expressed in terms of a set of single chance constraints as follows:

$$P\left(a_1\ x_1(t,\xi) \ge b_1\right) \le \eta_1,\dots,P\left(a_{n_C}\ x_{n_C}(t,\xi) \ge b_{n_C}\right) \le \eta_{n_C}, \tag{5}$$

where

$$\sum_{l=1}^{n_C} \eta_l = \eta. \tag{6}$$

Thus, the Bonferroni's inequality allows the joint chance constraint (4) to be split into multiple constraints of the form (5), in which the risk level is split among the n_C single chance constraints, according to the risk allocation (6).

3. Robust constrained optimal control

In the literature, there are two possible statements of a RCSOCP, which differ in the way the robust constraints are represented in terms of the expected value and standard deviation of the stochastic variables to be incorporated into the SOCP (1). The objective functional, the set of differential equations, and the boundary conditions are usually formulated as in the CCSOCP (2).

Let $C(t,\xi) \leq 0$ be an arbitrary stochastic constraint. In the first approach, the robustness of the constraint is expressed in terms of the following single constraint:

$$\mu(C(t,\xi)) + \kappa_C \cdot \sigma(C(t,\xi)) \leq 0, \tag{7}$$

where κ_C is a constant parameter that must be specified by the designers of the RCSOCP in order to adjust the probability of constraint satisfaction [47].

In the second approach, in which the stochastic constraint must be satisfied in the mean sense, the robustness is expressed in terms of two separate constraints as follows:

$$\mu(C(t,\xi)) \leq 0, \quad \sigma(C(t,\xi)) \leq \varepsilon_C, \tag{8}$$

where ε_C is a constant parameter that must be set by the designers of the RCOCP, which allows the dispersion of the constraint to be adjusted [48].

Similarly to chance constraints, robust constraints enable stochastic algebraic constraints to be included in the formulation of the SOCP (1), which permits the uncertainty management in the optimal control of stochastic epidemic models to be conducted. The effects of chance constraints and robust constraints on the solutions of SOCPs are compared and discussed in Sections 8 and 9.

4. Moment-based arbitrary polynomial chaos expansion

This section outlines the spectral technique employed to represent the propagation of the uncertainties, described by the random parameters $\xi = (\xi_1, \dots, \xi_{N_U})$, through the CCSOCP formulated in (2).

As explained in [49], multi-dimensional polynomial expansions can be computed, which represent surrogate models of the stochastic state variables $\mathbf{x}(t,\xi)$ of the CCSOCP stated in (2). More specifically, each component $x_l(t,\xi), l = 1, \dots, n$, of the vector of stochastic state variables $\mathbf{x}(t,\xi)$ can be approximated by a linear combination of N_P stochastic multivariate orthonormal polynomials $\boldsymbol{\Psi}^l_k(\xi)$ with deterministic coefficients $\alpha^l_k(t)$ as follows:

$$x_l(t,\xi) = x_l(t;\xi_1,\dots,\xi_{N_U}) \approx \sum_{k=1}^{N_P} \alpha^l_k(t) \cdot \boldsymbol{\Psi}^l_k(\xi_1,\dots,\xi_{N_U}), l = 1,\dots,n, \tag{9}$$

where $\xi = (\xi_1, \dots, \xi_{N_U})$ is assumed to be a vector of N_U independent random variables in the probability space $(\Omega, \Lambda, \Gamma)$ introduced in Section 2.1. Notice that each multivariate orthonormal polynomial $\boldsymbol{\Psi}^l_k(\xi)$, $k = 1, \dots, N_P$, $l = 1, \dots, n$, in (9) is computed as a product of univariate orthonormal polynomials $\psi^i_j(\xi_i)$, $i = 1, \dots, N_U$, $j = 1, \dots, p$, where index i refers to the components of the random vector parameter and index j refers to the order of the univariate orthonormal polynomial.

As a result of the orthonormality of the polynomials, the coefficients $\alpha^l_k(t)$, $k = 1, \dots, N_P$, $l = 1, \dots, n$, of the expansions (9) can be computed as

$$\alpha^l_k(t) = \int_{\xi\in\Omega} x_l(t,\xi)\Psi^l_k(\xi) d\Gamma(\xi). \tag{10}$$

In practice, different approaches can be followed in order to solve the integral (10), such as Galerkin projection, collocation, or numerical integration [50]. A Gaussian quadrature rule based on the statistical moments of $\xi = (\xi_1, \dots, \xi_{N_U})$ is used is this paper.

The full tensor product quadrature formula for a given multivariate function $\mathcal{F}(\xi)$ can be expressed as

$$\int_{c_1}^{d_1} \cdots \int_{c_{N_U}}^{d_{N_U}} \mathcal{F}(\xi)\, d\Gamma(\xi) \approx \sum_{i_1=1}^{p_1} \cdots \sum_{i_{N_U}=1}^{p_{N_U}} \mathcal{F}\left(\zeta^{i_1}, \dots, \zeta^{i_{N_U}}\right) \times \left(\omega_{i_1} \otimes \cdots \otimes \omega_{i_{N_U}}\right), \tag{11}$$

where ζ^{i_j} and $\omega_{i_j}, i = 1, \dots, p, j = 1, \dots, N_U$, respectively, are the nodes and weights of the numerical integration derived from the statistical moments of the random variables $\xi = (\xi_1, \dots, \xi_{N_U})$ [49]. Notice that, from a computational point of view, the full tensor Gaussian quadrature rule (11) becomes expensive when the number of random variables N_U grows. However, this drawback can be overcome by considering sparse grid quadrature rules, such as the Smolyak quadrature rule [51].

Polynomial expansions in which the optimal choices of the nodes and weights and the construction of the corresponding orthonormal polynomials are based on the statistical moments of the random variables are known as arbitrary Polynomial Chaos (aPC) expansions. The aPC approach provides a general framework that allows both random variables with known parametric probability distributions, such as continuous PDFs and discrete probability mass functions, and data sets with unknown parametric probability distributions to be taken into account [42].

5. Uncertainty management

The surrogate models represented by the polynomial expansions (9) provide a computational efficient approach to calculate the statistics of the stochastic vector of state variables $\mathbf{x}(t,\xi)$ of the CCSOCP (2). In particular, the expected value and variance of $x_l(t,\xi), l = 1, \dots, n$, can be formulated in terms of the coefficients $\alpha^l_k(t)$ as

$$\mu_{x_l} = \alpha^l_1(t) \quad \text{and} \quad \sigma^2_{x_l} = \sum_{k=2}^{N_P} \alpha^l_k(t)^2, \tag{12}$$

which can be efficiently calculated by means of scalar products of vectors using the quadrature rule (11) as follows:

$$\mu_{x_l} = x_l\left(t;\zeta^{i_1},\dots,\zeta^{i_{N_U}}\right)\cdot\boldsymbol{\omega} \quad \text{and} \quad \sigma^2_{x_l} = \left(x_l\left(t;\zeta^{i_1},\dots,\zeta^{i_{N_U}}\right) - \mu_{x_l}\right)^2\cdot\boldsymbol{\omega}, \tag{13}$$

where $\boldsymbol{\omega} = \left(\omega_{i_1},\dots,\omega_{i_{N_U}}\right)$ denotes the vector of Gaussian quadrature weights, with $i = 1, \dots, p$. Moreover, data smoothing problems can be formulated employing the surrogate models (9), which permit to compute kernel density estimations [52] of the marginals and joint PDFs and Cumulative Density Functions (CDFs) of the components of the stochastic vector of state variables $\mathbf{x}(t,\xi)$, at each time instant $t \in [t_I, t_F]$, with low computational cost.

Notice that, as explained in Section 6, the CCSOCP (2) can be reformulated through the surrogate models (9) by using the nodes and weights associated with the statistical moments of the random variables $\xi = (\xi_1, \dots, \xi_{N_U})$. In particular, the chance constraints (2c) can be reformulated in terms of μ_{x_l} and $\sigma^2_{x_l}$, $l = 1, \dots, n$, which allow the uncertainty management and risk analysis in the SOCP (1) to be carried out. Furthermore, a global sensitivity analysis, based on the variance of the optimal state variables $\mathbf{x}(t,\xi)$, can be conducted by means of the so-called Sobol' indices, which can also be computed in terms of the coefficients of the expansion (9) as described in [53,54].

6. Reformulation of the chance-constrained stochastic optimal control problem

The numerical resolution of the CCSOCP stated in (2) is based on the reformulation of the objective functional (2a), the stochastic differential Eqs. (2b), the chance constraint (2c), and the boundary conditions (2d), using the computational and statistical properties described in Sections 4 and 5 and provided by the surrogate models of the state variables represented by the aPC expansions (9).

The expected value and standard deviation of the objective functional (2a), which is assumed to be formulated in Mayer form by introducing a new state variable $x_{\mathcal{M}}(t,\boldsymbol{\xi})$, are expressed in terms of the coefficients of the polynomial expansion of $x_{\mathcal{M}}(t,\boldsymbol{\xi})$ using (12).

The stochastic differential equations (2b) are reformulated as a set of deterministic differential equations. Each of these deterministic differential equations is obtained by substituting the random parameter vector $\boldsymbol{\xi}=(\xi_1,\dots,\xi_{N_U})$ with each combination of the multivariate aPC nodes ζ^{i_j}, $i=1,\dots,p$, $j=1,\dots,N_U$.

In regard to the chance constraint, using the Chebyshev–Cantelli's inequality [55], it can be shown that the chance constraint (2c) is equivalent to the deterministic constraint

$$\mathbf{a}^2\ \boldsymbol{\mu}_{\mathbf{x}}+\boldsymbol{\kappa}_{\eta}\ \mathbf{a}\ \boldsymbol{\sigma}_{\mathbf{x}}\le\mathbf{b}, \tag{14}$$

with $\boldsymbol{\mu}_{\mathbf{x}}=(\mu_{x_1},\dots,\mu_{x_{n_C}})$, $\boldsymbol{\sigma}_{\mathbf{x}}=(\sigma_{x_1},\dots,\sigma_{x_{n_C}})$, and $\boldsymbol{\kappa}_{\eta}=(\kappa_{\eta_1},\dots,\kappa_{\eta_{n_C}})$, where the scalar parameter $\kappa_{\eta_l}=\sqrt{(1-\eta_l)/\eta_l}$, $l=1,\dots,n_C$, is referred to as safety parameter [56]. Therefore, according to (14), the chance constraints (3) can be algebraically rewritten in terms of the risk levels $\eta_l, l=1,\dots,n_C$, which are specified by the designers of the CCSOCP, and the first two moments of the state variables $x_l(t,\boldsymbol{\xi}), l=1,\dots,n$, which can be efficiently computed using (13). Moreover, notice that these reformulations of the chance constraints, which are expressed in terms of the expected value and the standard deviation of the state variables as in (7), are usually referred to as distributionally robust chance constraints [57].

Therefore, the chance constraints (2c) can be expressed in terms of the coefficients of the polynomial expansions of the state variables $\mathbf{x}(t,\boldsymbol{\xi})$ using (12). Similarly, the expected value and standard deviation of the boundary conditions (2d), can be expressed in terms of the coefficients of the polynomial expansions of the state variables using (12).

Let $\zeta^{i_1},\zeta^{i_2},\dots,\zeta^{i_{N_U}}$, $i=1,\dots,p$, be the set of nodes provided by the aPC expansions of order p of the stochastic state variables $\mathbf{x}(t,\boldsymbol{\xi})$ with respect to the random vector $\boldsymbol{\xi}=(\xi_1,\dots,\xi_{N_U})$. Then, the CCSOCP defined in (2) can be rewritten as follows:

$$\min_{\mathbf{u}(t)}\quad \alpha_{\mathcal{M}_1}(t_F)+\kappa_0\cdot\left(\sum_{k=2}^{N_P}\alpha^2_{\mathcal{M}_k}(t_F)\right)^{1/2}, \tag{15a}$$

subject to:

$$\dot{\mathbf{x}}_1(t,\boldsymbol{\xi}_1)=\mathbf{f}(\mathbf{x}(t,\boldsymbol{\xi}_1),\mathbf{u}(t),\boldsymbol{\xi}_1), \tag{15b}$$

$$\dot{\mathbf{x}}_2(t,\boldsymbol{\xi}_2)=\mathbf{f}(\mathbf{x}(t,\boldsymbol{\xi}_2),\mathbf{u}(t),\boldsymbol{\xi}_2), \tag{15c}$$

$$\cdots$$

$$\dot{\mathbf{x}}_p(t,\boldsymbol{\xi}_p)=\mathbf{f}(\mathbf{x}(t,\boldsymbol{\xi}_p),\mathbf{u}(t),\boldsymbol{\xi}_p), \tag{15d}$$

$$\mathbf{a}^2\ \boldsymbol{\alpha}_1(t)+\boldsymbol{\kappa}_{\eta}\ \mathbf{a}\left(\sum_{k=2}^{N_P}\boldsymbol{\alpha}_k^2(t)\right)^{1/2}\le\mathbf{b}, \tag{15e}$$

$$\boldsymbol{\alpha}_1(t_I)=\mathbf{x}_I,\ \left(\sum_{k=2}^{N_P}\boldsymbol{\alpha}_k^2(t_I)\right)^{1/2}\le\varepsilon_I,\ \boldsymbol{\alpha}_1(t_F)=\mathbf{x}_F,\ \left(\sum_{k=2}^{N_P}\boldsymbol{\alpha}_k^2(t_F)\right)^{1/2}\le\varepsilon_F, \tag{15f}$$

where $\boldsymbol{\xi}_i=(\zeta^{i_1},\dots,\zeta^{i_{N_U}})$, $i=1,\dots,p$, $\boldsymbol{\alpha}_k(t)=(\alpha_k^1(t),\dots,\alpha_k^n(t))$, $k=1,\dots,N_P$, and $\alpha_{\mathcal{M}_k}(t)$, $k=1,\dots,N_P$, are the coefficients of the aPC expansion of the state variable $x_{\mathcal{M}}(t,\boldsymbol{\xi})$ introduced to represent the objective functional (1a) in Mayer form.

Notice that the terms $\alpha_{\mathcal{M}_1}(t_F)$, $\sum_{k=2}^{N_P}\alpha^2_{\mathcal{M}_k}(t_F)$, $\boldsymbol{\alpha}_1(t)$, and $\sum_{k=2}^{N_P}\boldsymbol{\alpha}_k^2(t)$ are deterministic functions of time t. Therefore, according to (15b)–(15d), the CCSOCP (2) is converted into an augmented deterministic OCP, in which particular instances of the ODE system, corresponding to the nodes of the random variables, are combined into a single OCP. Thus, (15) is a deterministic OCP, which can be solved using traditional numerical techniques for the resolution of deterministic continuous OCPs. In particular, in this paper, the Hermite–Simpson direct collocation method is used [58].

7. Application to the COVID-19 pandemic

To illustrate the practical implementation of the proposed approach, the chance-constrained optimal control of a COVID-19 epidemic model has been considered in this paper.

7.1. Mathematical model of COVID-19 transmission

The considered epidemic model, denoted as SEIsIaQRS, has 6 compartments. It is schematically shown in Fig. 1 and represented by the following set of ODEs:

$$\dot{S}(t) = -\frac{\theta}{T_{inf}}(1-\varepsilon\upsilon(t))\frac{I_s(t)+\alpha I_a(t)}{N(t)}S(t)-\varepsilon\upsilon(t)S(t)+\delta R(t), \tag{16a}$$

$$\dot{E}(t) = \frac{\theta}{T_{inf}}(1-\varepsilon\upsilon(t))\frac{I_s(t)+\alpha I_a(t)}{N(t)}S(t)-\frac{E(t)}{T_{lat}}, \tag{16b}$$

$$\dot{I}_s(t) = (1-\beta)\frac{E(t)}{T_{lat}}-\left(\kappa_s+\frac{1}{T_{inf}}\right)I_s(t), \tag{16c}$$

$$\dot{I}_a(t) = \beta\frac{E(t)}{T_{lat}}-\left(\kappa_a(t)+\frac{1}{T_{inf}}\right)I_a(t), \tag{16d}$$

$$\dot{Q}(t) = \kappa_s I_s(t)+\kappa_a(t)I_a(t)-\frac{Q(t)}{T_{ser}}, \tag{16e}$$

$$\dot{R}(t) = \frac{I_s(t)+I_a(t)}{T_{inf}}+\frac{Q(t)}{T_{ser}}+\varepsilon\upsilon(t)S(t)-\delta R(t). \tag{16f}$$

The state variables $S(t)$, $E(t)$, $I_s(t)$, $I_a(t)$, $Q(t)$, and $R(t)$ of the ODE system (16) correspond to the number of susceptible, exposed, symptomatic, asymptomatic, isolated, and recovered subjects, respectively, whereas the state variable $N(t)$ corresponds to the total population. Moreover, the mass conservation property is assumed, namely

$$N(t)=S(t)+E(t)+I_s(t)+I_a(t)+Q(t)+R(t),\qquad \text{for all } t\in[t_I,t_F].$$

The control variables $\upsilon(t)$ and $\kappa_a(t)$ of the ODE system (16) correspond to the vaccination rate for the immunization of susceptible subjects and the testing rate for the identification and isolation of asymptomatic infected subjects, respectively. The control variable $\upsilon(t)$ ranges from 0 to υ_U, whereas the control variable $\kappa_a(t)$ ranges from 0 to κ_U, where υ_U and κ_U are upper bounds that must be set by the designers of the CCSOCP.

The meaning of the parameters of the ODE system (16) and their corresponding values are summarized in Table 1.

According to [59], the ratio between infectiousness of asymptomatic and symptomatic subjects has been set to $\alpha=1$, whereas, according to [60], the population ratio that remains asymptomatic has been set to $\beta=0.8$. Following [45,59], the isolation rate of symptomatic subjects has been set to $\kappa_s=0.95$. According to [65,66], the mean serial time interval, the mean incubation period, and the infectious period have been set to $T_{ser}=7.5$, $T_{lat}=5.2$, and $T_{inf}=2.3$ days, respectively.

It has been assumed that the social distancing measures have been barely applied. Therefore, following [54] and according to the sensitivity analysis conducted in [60], the replication factor, θ, has been supposed to be a random variable centred at 3.5. More specifically, the random parameter θ has been modelled using a gamma distribution G(3500, 0.001). Moreover, according to the vaccine efficacy reported in [64,67,68] and following the sensitivity analysis conducted in [45], the vaccine efficacy, ε, has been assumed to be a random variable

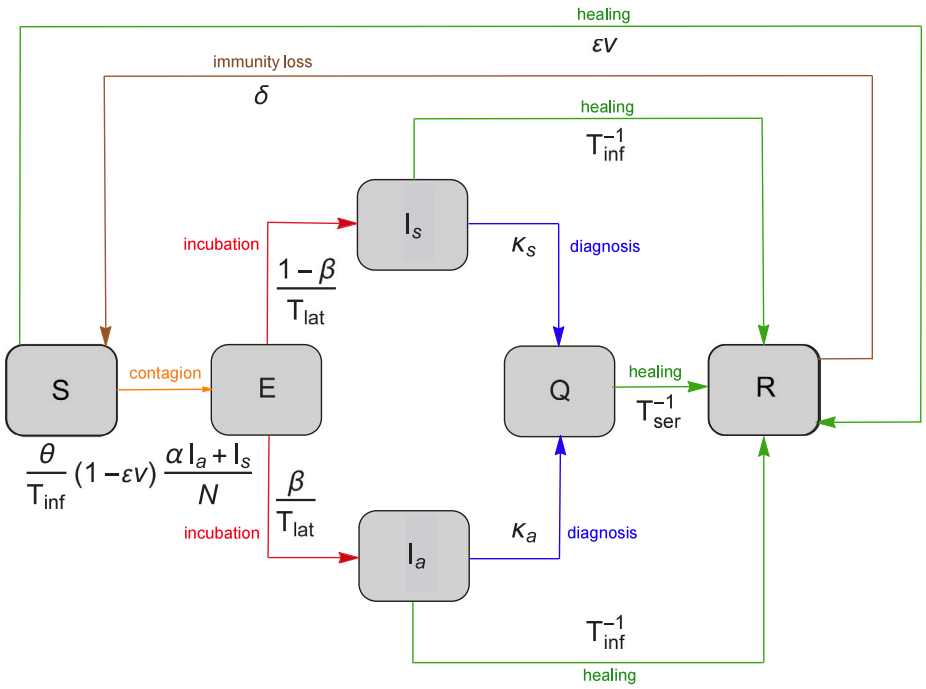

Fig. 1. Schematic representation of the SEIsIaQRS compartmental model with immunity loss and vaccination and testing strategies.

Table 1
Values of the parameters of the SEIsIaQRS model used in the numerical experiments.

Parameter	Meaning	Value	Units	Source
α	Asymptomatic over symptomatic subjects ratio	1.000	dimensionless	[59]
β	Population ratio that remains asymptomatic	0.800	dimensionless	[60]
δ	Immunity loss	Random	days^{-1}	[61–63]
ε	Vaccine efficacy	Random	dimensionless	[45,64]
κ_s	Isolation rate of symptomatic subjects	0.950	dimensionless	[45,59]
θ	Replication factor	Random	dimensionless	[54,60]
T_{ser}	Mean serial time interval	7.500	days	[65]
T_{lat}	Mean incubation period	5.200	days	[65,66]
T_{inf}	Mean infectious period	2.300	days	[66]

centred at 0.95. More specifically, the random parameter ε has been modelled using a beta distribution B(160, 10). Finally, according to different works, which have reported a duration of the immunity ranging from 6 months [61] to 3 years [62], and following the sensitivity analysis conducted in [63], the immunity loss, δ, has been assumed to be a random variable centred at 0.0028. More specifically, the random parameter δ has been modelled using a beta distribution B(160, 10).

Notice that, in model (16), the term $\varepsilon v(t)S(t)$ represents the vaccination policy, with parameter ε being the vaccine efficacy level. Only the susceptible subjects are assumed to be vaccinated. Moreover, the term $\kappa_a(t)I_a(t)$ represents the testing strategy for the detection of asymptomatic infected subjects.

Thus, in this application, a CCSOCP based on the ODE system (16) is formulated, in which the effects on the transmission of the disease of the uncertainty on the replication factor, the immunity loss, and the vaccine efficacy represented by parameters θ, δ, and ε, respectively, are quantified and managed.

7.2. Chance-constrained stochastic optimal control of COVID-19 transmission

Different strategies to control the spread of COVID-19 represented by the model (16) can be obtained depending on the objective functional and the constraints considered.

Assume that the objective functional to be minimized is a combination of the number of infectious subjects and the overall cost of the vaccination and testing during a fixed time period $[t_I, t_F]$, namely

$$\mathcal{J}(I_s(t), I_a(t), v(t), \kappa_a(t)) = \int_{t_I}^{t_F} \left(C_1 \cdot I_s(t) + C_2 \cdot I_a(t) + C_3 \cdot v^2(t) + C_4 \cdot \kappa_a^2(t)\right) dt, \tag{17}$$

where $C_i, i = 1, 2, 3, 4$, are weighting parameters that must be set by the designers of the CCSOCP. Additionally, for all $t \in [t_I, t_F]$, assume that the following constraint is considered:

$$I_a(t) \leq I_{a_U}, \tag{18}$$

where parameter I_{a_U} denotes an upper bound on the number of daily asymptomatic infected subjects. Then, the chance-constrained stochastic optimal control of the SEIsIaQRS compartmental model (16) with objective functional (17) and algebraic constraint (18) is stated as follows:

$$\min_{v(t),\kappa_a(t)} \quad M_{\mathcal{J}}(t,\xi) + \kappa_0 \cdot \Sigma_{\mathcal{J}}(t,\xi) \tag{19a}$$

subject to:

$$\dot{S}(t,\xi) = -\frac{\theta}{T_{inf}}(1-\varepsilon v(t))\frac{I(t,\xi)}{N}S(t,\xi) - \varepsilon v(t)S(t,\xi) + \delta R(t,\xi) \text{ a.s.,} \tag{19b}$$

$$\dot{E}(t,\xi) = \frac{\theta}{T_{inf}}(1-\varepsilon v(t))\frac{I(t,\xi)}{N}S(t,\xi) - \frac{E(t,\xi)}{T_{lat}} \text{ a.s.,} \tag{19c}$$

$$\dot{I}_s(t,\xi) = (1-\beta)\frac{E(t,\xi)}{T_{lat}} - \left(\kappa_s + \frac{1}{T_{inf}}\right) I_s(t,\xi) \text{ a.s.,} \tag{19d}$$

$$\dot{I}_a(t,\xi) = \beta\frac{E(t,\xi)}{T_{lat}} - \left(\kappa_a(t) + \frac{1}{T_{inf}}\right) I_a(t,\xi) \text{ a.s.,} \tag{19e}$$

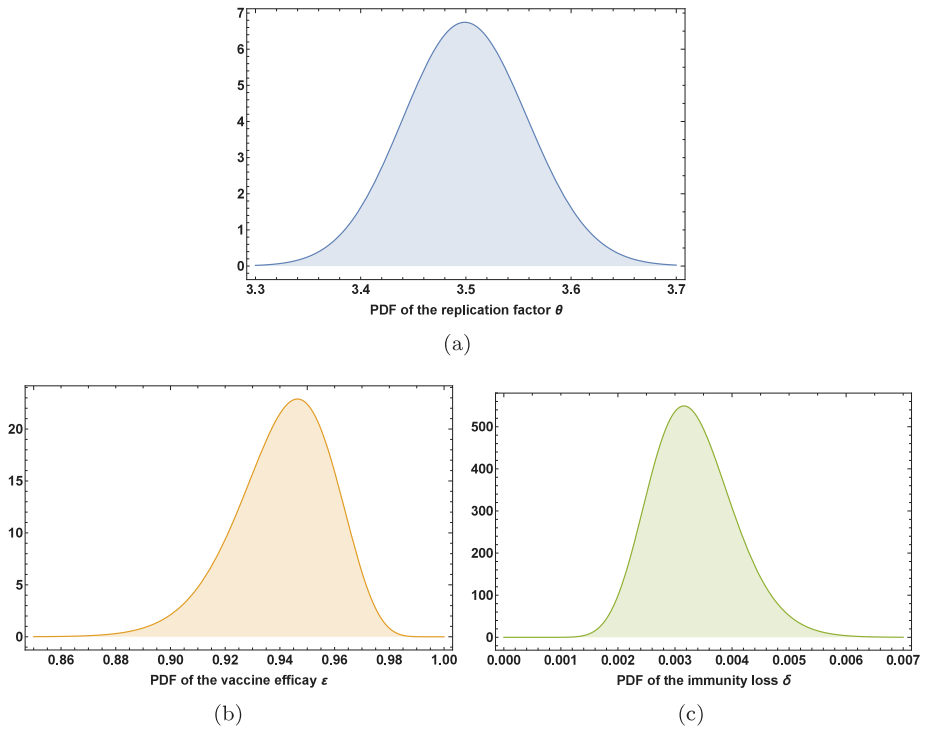

Fig. 2. PDFs of the random parameters $\xi = (\theta, \varepsilon, \delta)$ of the CCSOCP (19).

$$\dot{Q}(t,\xi) = \kappa_s I_s(t,\xi) + \kappa_a(t) I_a(t,\xi) - \frac{Q(t,\xi)}{T_{ser}} \text{ a.s.}, \tag{19f}$$

$$\dot{R}(t,\xi) = \frac{I_s(t,\xi) + I_a(t,\xi)}{T_{inf}} + \frac{Q(t,\xi)}{T_{ser}} + \varepsilon \upsilon(t) S(t,\xi) - \delta R(t,\xi) \text{ a.s.}, \tag{19g}$$

$$P\left(I_a(t,\xi) \le I_{a_U}\right) \ge 1 - \eta_a, \tag{19h}$$

$$\mu\left(S(t_I,\xi)\right) = S_I, \quad \mu\left(E(t_I,\xi)\right) = E_I, \quad \mu\left(I_s(t_I,\xi)\right) = I_{s_I}, \tag{19i}$$

$$\mu\left(I_a(t_I,\xi)\right) = I_{a_I}, \quad \mu\left(Q(t_I,\xi)\right) = Q_I, \quad \mu\left(R(t_I,\xi)\right) = R_I, \tag{19j}$$

$$\sigma\left(S(t_I,\xi)\right) \le \varepsilon_I, \quad \sigma\left(E(t_I,\xi)\right) \le \varepsilon_I, \quad \sigma\left(I_s(t_I,\xi)\right) \le \varepsilon_I, \tag{19k}$$

$$\sigma\left(I_a(t_I,\xi)\right) \le \varepsilon_I, \quad \sigma\left(Q(t_I,\xi)\right) \le \varepsilon_I, \quad \sigma\left(R(t_I,\xi)\right) \le \varepsilon_I, \tag{19l}$$

where $I(t,\xi) = I_s(t,\xi) + \alpha I_a(t,\xi)$, $M_{\mathcal{J}}(t,\xi) = \mu\left(\mathcal{J}(I_s(t,\xi), I_a(t,\xi), \upsilon(t), \kappa_a(t), \xi)\right)$, and $\Sigma_{\mathcal{J}}(t,\xi) = \sigma\left(\mathcal{J}(I_s(t,\xi), I_a(t,\xi), \upsilon(t), \kappa_a(t), \xi)\right)$, with $\upsilon(t) \in [0, \upsilon_U]$, $\kappa_a(t) \in [0, \kappa_U]$, $\xi = (\theta, \varepsilon, \delta)$, and $\mathcal{J}(\cdot)$ defined as in (17).

8. Numerical experiments

To show the practical application of the proposed approach to the uncertainty management in epidemic models, based on the formulation of CCSOCPs, various numerical experiments have been carried out, in which the mathematical model of COVID-19 transmission introduced in Section 7.1 has been used.

In all these experiments, it has been assumed that $N(t) = 1$, namely a non-dimensionalized version of the SEIsIaQRS model (16) has been employed, so that all the state variables have the same order of magnitude. This scaling of variables allows computational issues that could arise when numerically solving the CCSOCP (19) to be prevented. Moreover, following [45], the initial conditions at time instant $t = 0$ have been set to:

$$(S_0 = 0.84908, E_0 = 0.00102, I_{s_0} = 0.0002,$$
$$I_{a_0} = 0.0008, Q_0 = 0, R_0 = 0.1489).$$

Furthermore, as mentioned above, it has been assumed that the replication factor θ follows a gamma distribution G(3500, 0.001), the vaccine efficacy ε follows a beta distribution B(160, 10), and the immunity loss rate δ follows a beta distribution B(20, 6000), as shown in Fig. 2. These random parameters have been modelled using an aPC expansion of order $p = 4$ and the upper bound for the standard deviations in the boundary conditions (19k)–(19l) has been set to $\varepsilon_I = 10^{-6}$. Additionally, the upper bounds on the vaccination and testing rates have been set to $\upsilon_U = 0.007$ and $\kappa_U = 0.5$, respectively, whereas the weighting parameters of the objective functional (17) have been set to $C_1 = 0.15, C_2 = 0.095, C_3 = 0.75$, and $C_4 = 0.005$.

Notice that the values of the parameters considered in these experiments are not intended to represent a specific current scenario. They have been chosen with the aim of illustrating the practical application of the proposed methodology for academic purposes only.

8.1. Experiment 1: Single chance constraint

In this experiment, the CCSOCP (19) is solved for $I_{a_U} = 0.006$ and $\eta_a = 0.05$. Fig. 3 shows in green lines the expected values of the obtained optimal state variables, together with their 2-sigma confidence envelopes. The corresponding optimal control variables, which represent the vaccination and testing rates, are represented in Fig. 4. The proportions of susceptible vaccinated subjects and asymptomatic tested subjects, namely $\upsilon(t)S(t)$ and $\kappa_a(t)I_a(t)$, respectively, are shown for every $t \in [t_I, t_F]$ in Fig. 5. These will be referred to as the vaccination and testing policies. For the sake of comparison, Figs. 3 and 4 also show in red lines the optimal state and control variables obtained when the chance constraint (19h) is removed. The corresponding proportions of susceptible vaccinated subjects and asymptomatic tested subjects are represented in Fig. 5 as well.

As it can be seen in Fig. 3, the development of the outbreak of the infectious disease changes considerably when the single chance constraint (19h) is imposed. More specifically, as shown in Fig. 3c, around day 48 the 2-sigma confidence envelope for the proportion of symptomatic infected subjects represented in green reaches a peak of (0.0004, 0.0007)%, whereas this peak rises to (0.0007, 0.0011)% for the envelope represented in red, which means a significant increase in the proportion of symptomatic infected subjects when the chance constraint (19h) is not taken into account. Similar differences can be noticed in the evolution of the 2-sigma confidence envelopes for the

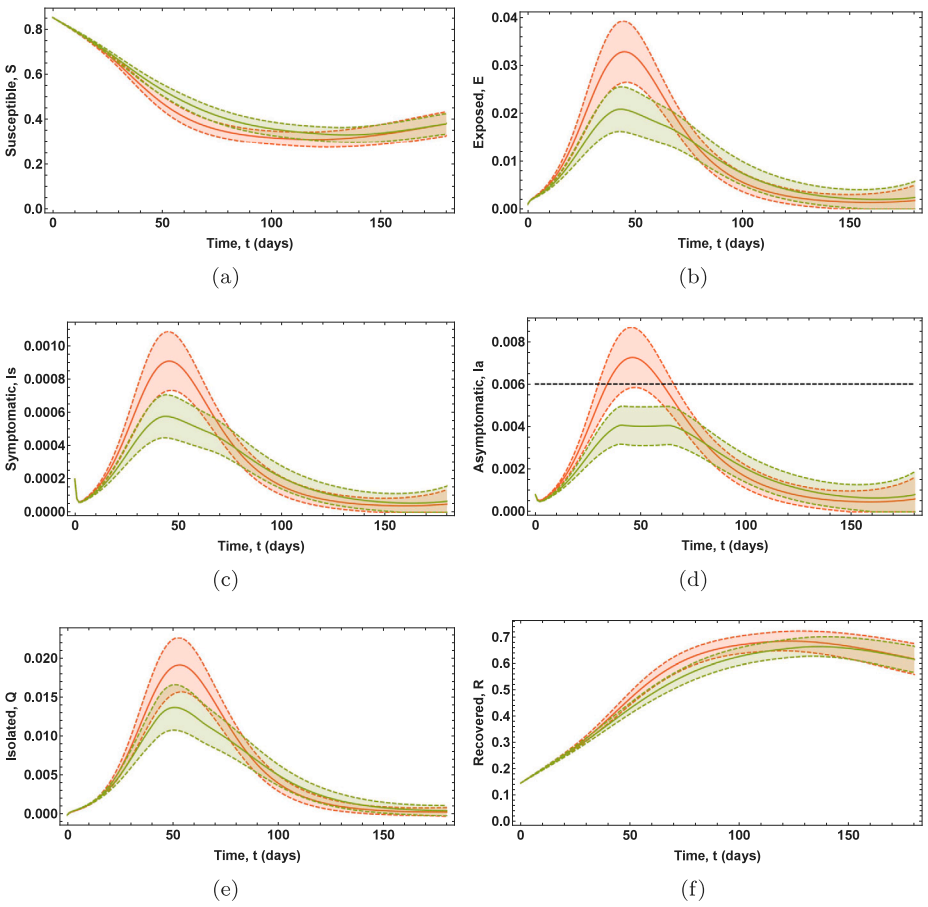

Fig. 3. Experiment 1. Expected values of the proportions of subjects in each compartment, together with their 2-sigma confidence envelopes. The curves corresponding to the solutions obtained with and without the single chance constraint are shown in green and red, respectively. The 2-sigma confidence envelope for the proportion of asymptomatic subjects represented in green clearly remains below the preset threshold of 0.006, due to the effect of the chance constraint (19h). (For interpretation of the references to colour in this figure legend, the reader is referred to the web version of this article.)

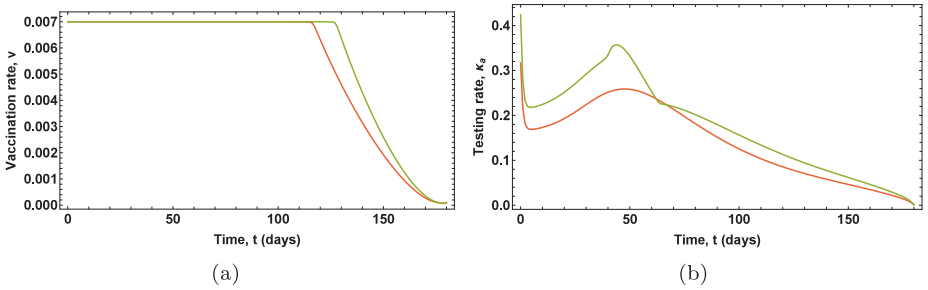

Fig. 4. Experiment 1. Optimal vaccination and testing rates. The curves corresponding to the solutions obtained with and without the single chance constraint are shown in green and red, respectively. The effect of the chance constraint (19h) is mainly achieved through the increase in the testing and isolation of asymptomatic subjects during the first 60 days. (For interpretation of the references to colour in this figure legend, the reader is referred to the web version of this article.)

proportion of exposed and isolated subjects, as shown in Fig. 3b and e, respectively. The effect of these differences can be observed in the behaviour of the 2-sigma confidence envelope for the proportion of both susceptible and recovered subjects between day 50 and day 100, as shown in Fig. 3a and f, respectively.

The direct effect of the chance constraint (19h) can be seen in Fig. 3d, in which the 2-sigma confidence envelope for the proportion of asymptomatic subjects clearly remains below the preset threshold of 0.006. This effect is mainly due to the increase in the testing and isolation of asymptomatic subjects during the first 60 days, as shown in Fig. 4b, which, as mentioned before, turns into a greater reduction of the proportion of exposed, symptomatic, and isolated subjects, as can be seen in Fig. 3b, c, and e, respectively. Therefore, a greater screening of asymptomatic subjects ultimately results in a greater reduction of the disease transmission.

8.2. Experiment 2: Single robust constraint

In this experiment, the single chance constraint (19h) is replaced by the single robust constraint

$$\mu(I_a(t,\xi)) + \kappa_{a_C} \cdot \sigma(I_a(t,\xi)) \leq I_{a_U}, \tag{20}$$

with $I_{a_U} = 0.006$ and $\kappa_{a_C} = 2$, whereas the rest of the expressions are the same as in Experiment 1. The presence of this constraint converts the CCSOCP (19) into a RCSOCP, with a single robust constraint of the form (7), as described in Section 3.

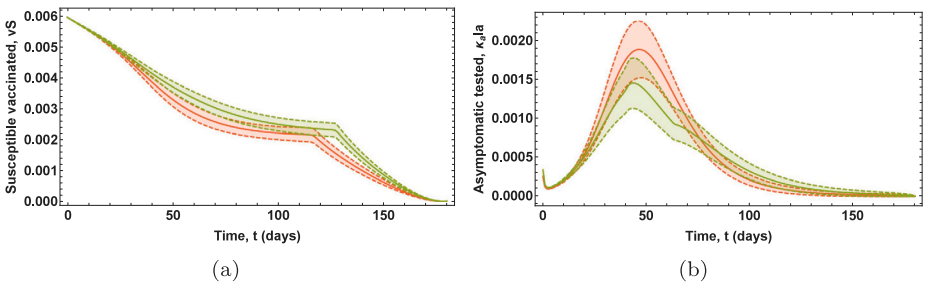

Fig. 5. Experiment 1. Expected values of the proportion of susceptible vaccinated subjects and asymptomatic tested subjects, together with their 2-sigma confidence envelopes. The curves corresponding to the solutions obtained with and without the single chance constraint are shown in green and red, respectively. The chance constraint (19h) implies an overall increase in the vaccination policy and a decrease in the testing policy during the first 60 days. (For interpretation of the references to colour in this figure legend, the reader is referred to the web version of this article.)

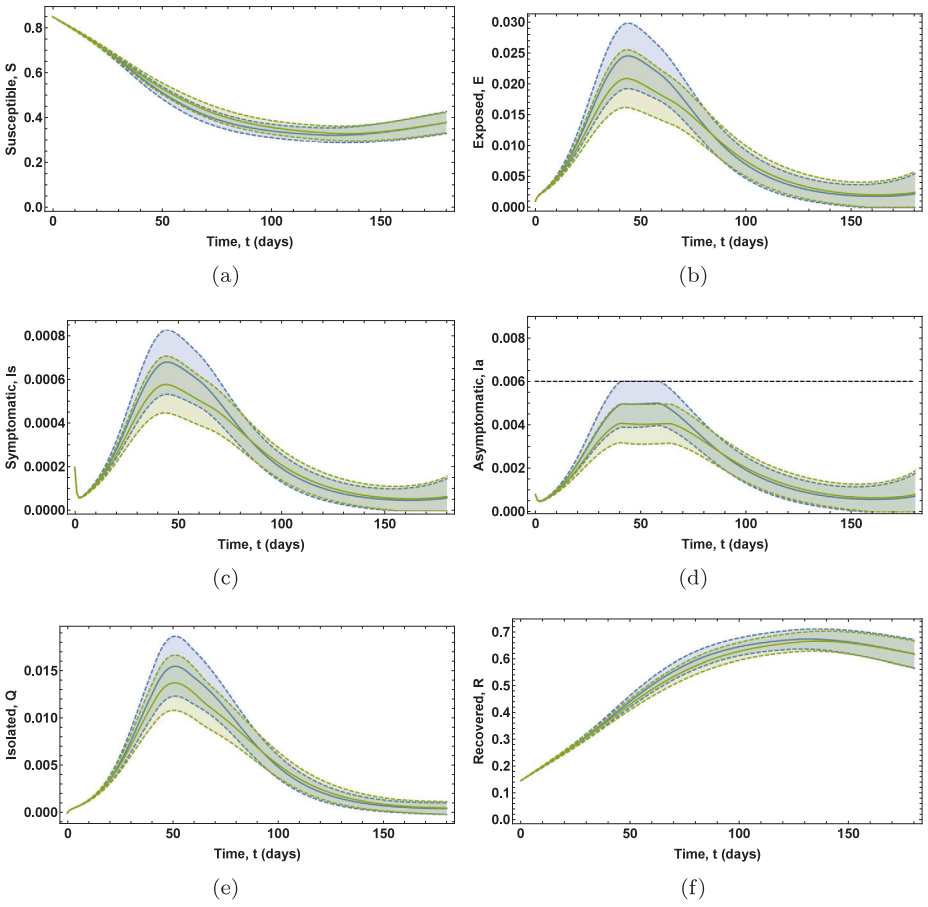

Fig. 6. Experiment 2. Expected values of the proportions of subjects in each compartment, together with their 2-sigma confidence envelopes. The curves corresponding to the solutions obtained with the single robust constraint and the single chance constraint are shown in blue and green, respectively. The 2-sigma confidence envelope for the proportion of asymptomatic subjects in the RCSOCP reaches the preset threshold of 0.006, namely the single robust constraint (20) is saturated, meaning that the threshold violation probability is greater when the single robust constraint is considered. (For interpretation of the references to colour in this figure legend, the reader is referred to the web version of this article.)

Fig. 6 shows in blue lines the expected values of the optimal state variables, together with their 2-sigma confidence envelopes, obtained in the solution of this RCSOCP. The associated optimal control variables are represented in Fig. 7, whereas the corresponding vaccination and testing policies are shown in Fig. 8. For the sake of comparison, Figs. 6, 7, and 8 also show in green lines the optimal state and control variables, as well as the corresponding vaccination and testing strategies, obtained in the solution of the CCSOCP considered in Experiment 1.

As in the case of the single chance constraint, the effect of the single robust constraint can be clearly seen in Fig. 6. However, as shown in Fig. 7, there are slight differences in the behaviour of the optimal control variables, mainly in the testing and isolation of asymptomatic subjects during the first 60 days, in which the testing rate is lower when the single robust constraint is considered. These differences lead to a noticeable change in the evolution of the proportion of asymptomatic subjects, as can be seen in Fig. 6d. More specifically, unlike in the case of the solution of the CCSOCP, the 2-sigma confidence envelope for the proportion of asymptomatic subjects in the RCSOCP reaches the preset threshold of 0.006, namely the single robust constraint (20) is saturated, meaning that the threshold violation probability is greater when the single robust constraint is considered.

It is well known that a significant percentage of the realizations of a random variable is not included in a 2-sigma confidence interval. For instance, this percentage is approximately 5% for a Gaussian random

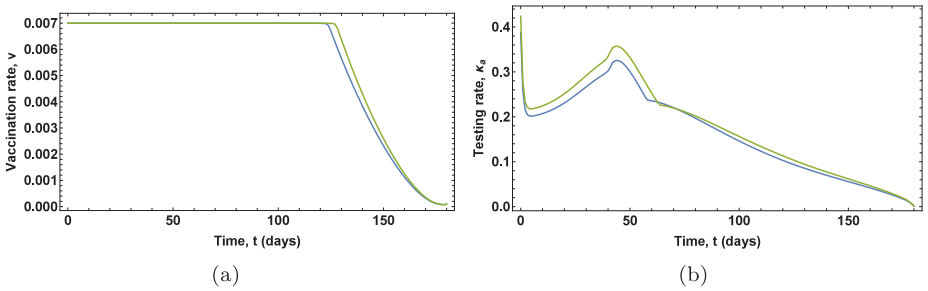

Fig. 7. Experiment 2. Optimal vaccination and testing rates. The curves corresponding to the solutions obtained with the single robust constraint and the single chance constraint are shown in blue and green, respectively. There are slight differences in the behaviour of the optimal control variables, mainly in the testing and isolation of asymptomatic subjects during the first 60 days, in which the testing rate is lower when the single robust constraint is considered. (For interpretation of the references to colour in this figure legend, the reader is referred to the web version of this article.)

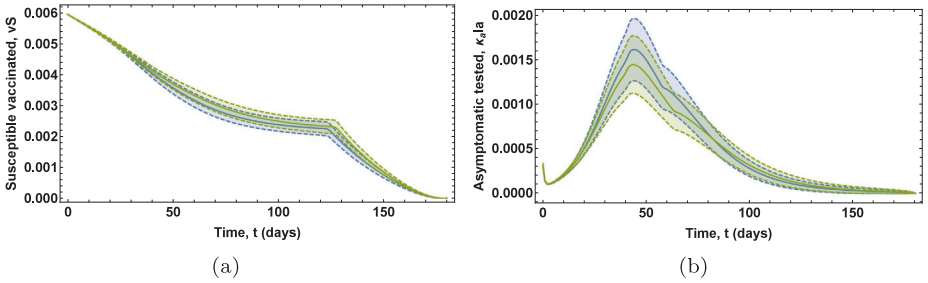

Fig. 8. Experiment 2. Expected values of the proportion of susceptible vaccinated subjects and asymptomatic tested subjects, together with their 2-sigma confidence envelopes. The curves corresponding to the solutions obtained with the single robust constraint and the single chance constraint are shown in blue and green, respectively. The vaccination policies are similar, whereas the testing policy during the first 60 days is slightly higher when the single robust constraint is considered. (For interpretation of the references to colour in this figure legend, the reader is referred to the web version of this article.)

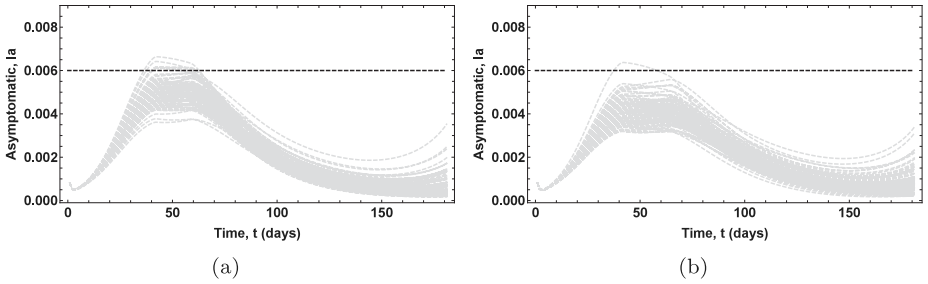

Fig. 9. Experiment 2. MC simulations of the proportion of asymptomatic subjects obtained with the single robust constraint (left) and the single chance constraint (right). In the case of the single chance constraint, the threshold is violated in 0.10% of the samples, whereas this percentage rises to 4.15% in the case of the single robust constraint.

variable. However, each optimal state variable observed at an arbitrary time instant $t \in [t_I, t_F]$ can have an arbitrary PDF. Therefore, if the single robust constraint (20) is saturated in the solution of the RCSOCP, then the actual threshold violation probability is not known. Notice that, although the chance constraint (19h) is not saturated, the actual threshold violation probability is not known either in the case of the CCSOCP, since the chance constraint only provides a lower bound for the constraint satisfaction probability at each time instant.

The surrogate model provided by the aPC expansion (9) allows the actual threshold violation probability to be estimated by means of a MC simulation. In particular, MC simulations with 10 000 runs have been done using the surrogate models of the optimal proportion of asymptomatic subjects obtained in the solutions of both the CCSOCP and the RCSOCP as shown in Fig. 9, in which, for the sake of clarity, only the results of 100 runs are reported. According to the MC simulations, in the CCSOCP, the threshold is violated in 0.10% of the samples, whereas this percentage rises to 4.15% in the RCSOCP.

Moreover, as explained in Section 5, the surrogate model (9) also allows the PDF of the optimal state variables at each time instant $t \in [t_I, t_F]$ to be estimated. The availability of these PDFs enables a wide range of statistical analyses to be conducted. In particular, the threshold violation probability can be computed at each time instant for the proportion of asymptomatic subjects. More specifically, the PDFs of $I_a(t, \xi)$ at time instants $t = 30$, $t = 40$, $t = 50$, $t = 60$, and $t = 70$ days have been estimated using a Gaussian kernel estimator, which are shown in Fig. 10 for both the CCSOCP and the RCSOCP. For instance, at time instant $t = 50$ days, the threshold violation probability in the CCSOCP is $P(I_a(50, \xi) > 0.006) = 0.00004$, whereas in the RCSOCP this probability rises to 0.03628.

8.3. Experiment 3: Separate robust constraints

In this experiment, the single chance constraint (19h) is replaced by the separate robust constraints

$$\mu(I_a(t, \xi)) \leq I_{a_U}, \quad \sigma(I_a(t, \xi)) \leq \varepsilon_{a_C}, \tag{21}$$

with $I_{a_U} = 0.006$ and $\varepsilon_{a_C} = 0.0002$, whereas the rest of the expressions are the same as in Experiment 1. The presence of these constraints converts the CCSOCP (19) into a RCSOCP, with two separate robust constraints of the form (8), as described in Section 3.

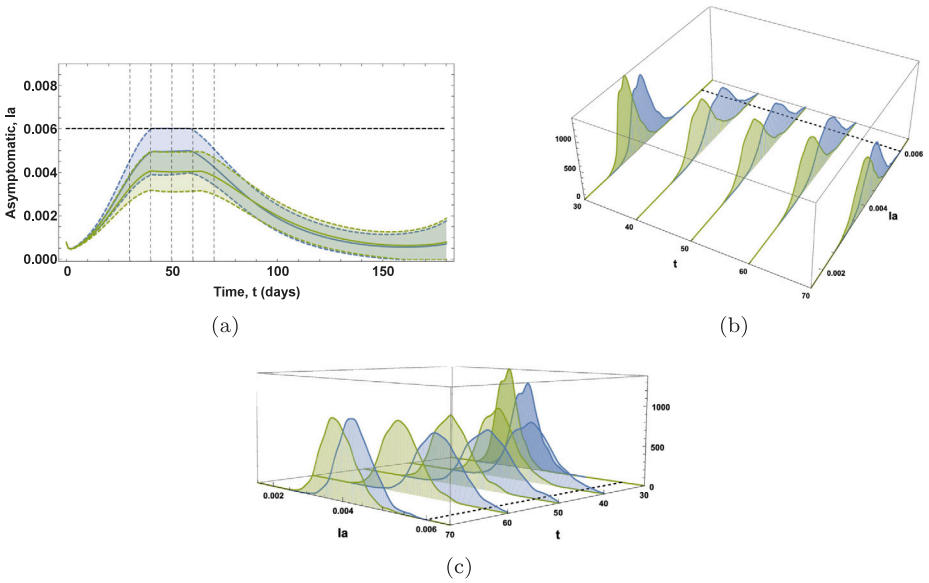

Fig. 10. Experiment 2. PDFs of the proportion of asymptomatic subjects at time instants $t = 30$, $t = 40$, $t = 50$, $t = 60$, and $t = 70$ days. The PDFs corresponding to the solutions obtained with the single robust constraint and the single chance constraint are shown in blue and green, respectively. At time instant $t = 50$ days, the threshold violation probability in the case of the single chance constraint is 0.00004, whereas in the case of the single robust constraint, this probability rises to 0.03628. (For interpretation of the references to colour in this figure legend, the reader is referred to the web version of this article.)

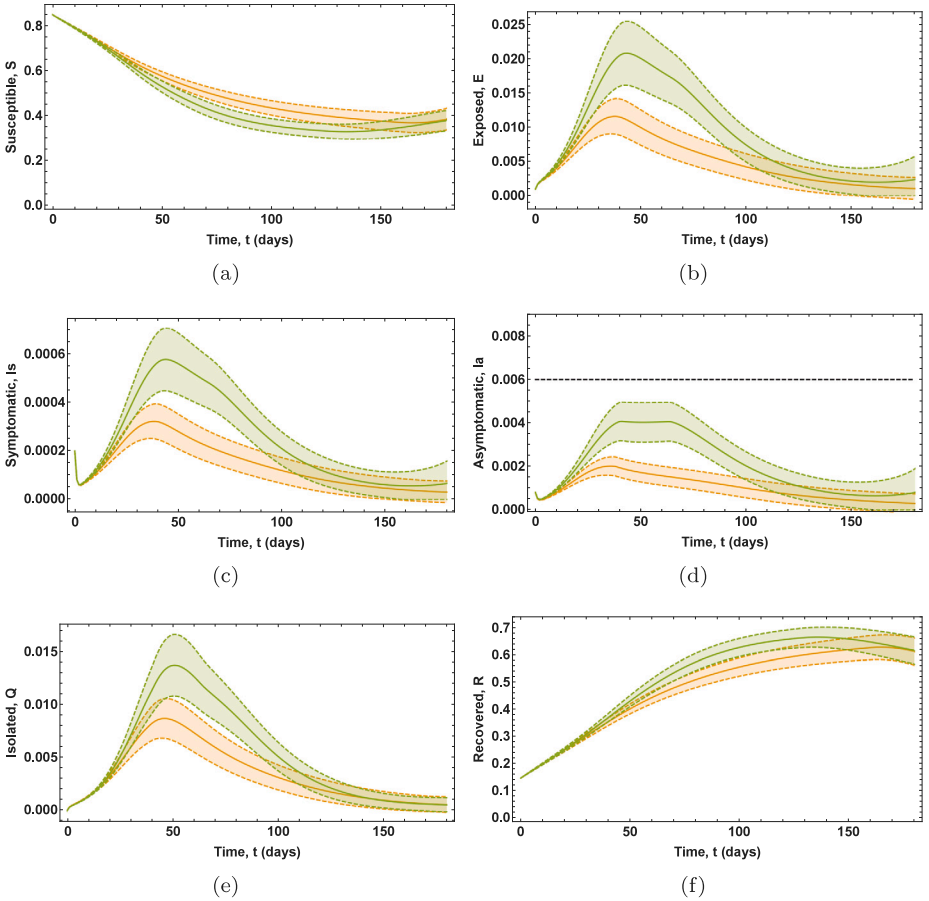

Fig. 11. Experiment 3. Expected values of the proportions of subjects in each compartment, together with their 2-sigma confidence envelopes. The curves corresponding to the solutions obtained with the separate robust constraints and the single chance constraint are shown in orange and green, respectively. The 2-sigma confidence envelopes for the proportion of exposed, symptomatic, asymptomatic, and isolated subjects are clearly lower when the separate robust constraints are considered. However, this result is achieved at the cost of increasing significantly the needed vaccine and testing supplies. (For interpretation of the references to colour in this figure legend, the reader is referred to the web version of this article.)

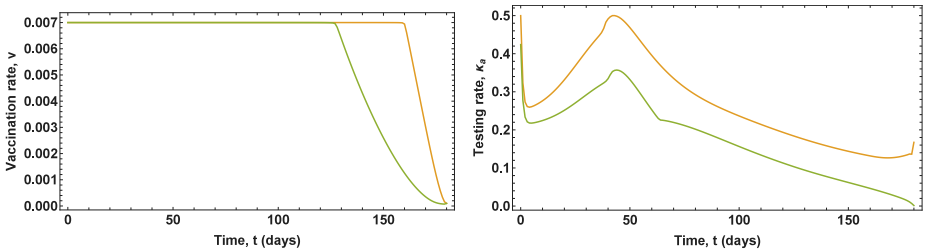

(a) (b)

Fig. 12. Experiment 3. Optimal vaccination and testing rates. The curves corresponding to the solutions obtained with the separate robust constraints and the single chance constraint are shown in orange and green, respectively. The effect of the separate robust constraints is achieved through an overall increase in the testing and isolation of asymptomatic subjects. Moreover, the maximum daily vaccination rate must be scheduled almost during the whole time period under consideration. (For interpretation of the references to colour in this figure legend, the reader is referred to the web version of this article.)

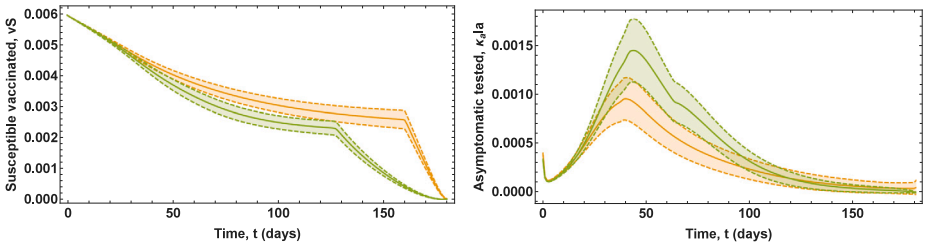

(a) (b)

Fig. 13. Experiment 3. Expected values of the proportion of susceptible vaccinated subjects and asymptomatic tested subjects, together with their 2-sigma confidence envelopes. The curves corresponding to the solutions obtained with the separate robust constraints and the single chance constraint are shown in orange and green, respectively. The separate robust constraints imply an overall increase in the vaccination policy and a decrease in the testing policy during the first 90 days. (For interpretation of the references to colour in this figure legend, the reader is referred to the web version of this article.)

Fig. 11 shows in orange lines the expected values of the optimal state variables, together with their 2-sigma confidence envelopes, obtained in the solution of this RCSOCP. The associated optimal control variables are represented in Fig. 12, and the corresponding vaccination and testing policies are shown in Fig. 13. For the sake of comparison, Figs. 11, 12, and 13 also show in green lines the optimal state and control variables, as well as the corresponding vaccination and testing strategies, obtained in the solution of the CCSOCP considered in Experiment 1.

It can be seen in Fig. 12 that the behaviour of the optimal control variables obtained in the solution of the RCSOCP with separate robust constraints noticeably differ from the optimal control variables obtained in the solution of the CCSOCP, which leads to considerable differences in the evolution of the optimal state variables represented in Fig. 11. More specifically, compared to the CCSOCP solved in Experiment 1, the 2-sigma confidence envelopes for the proportion of exposed, symptomatic, asymptomatic, and isolated subjects are clearly lower when the separate robust constraints are considered, meaning a better outcome from the point of view of the control of the disease transmission. However, this result is achieved at the cost of increasing significantly the needed vaccine and testing supplies. Indeed, according to the optimal control variables, the maximum daily vaccination rate should be scheduled almost during the whole time period under consideration, as shown in Fig. 12a.

It is important to point out the lack of predictability of the evolution of the optimal state variables when the separate robust constraints are considered. Unlike in the previous experiments, due to the constraint on the standard deviation $\sigma(I_a(t,\xi)) \leq \varepsilon_{a_C}$, it is not possible to know in advance an estimate of the threshold violation probability. Indeed, for larger values of ε_{a_C}, the threshold can be clearly violated by the 2-sigma confidence envelope, since only the expected value of the proportion of asymptomatic subjects is assumed to remain below the threshold.

8.4. Experiment 4: Joint chance constraint

In this experiment, the single chance constraint (19h) is replaced by the joint constraint

$$P\left(I_s(t,\xi) \leq I_{s_U}, I_a(t,\xi) \leq I_{a_U}\right) \geq 1-\eta, \tag{22}$$

with $I_{s_U} = 0.0006$ and $I_{a_U} = 0.006$, whereas the rest of the expressions are the same as in Experiment 1. The joint chance constraint (22) included in the formulation of the CCSOCP (19) is of the form (4). As described in Section 2.3, the Bonferroni's inequality allows the joint chance constraint (22) to be split into the single chance constraints

$$P\left(I_s(t,\xi) \geq I_{s_U}\right) \leq \eta_s, \quad P\left(I_a(t,\xi) \geq I_{a_U}\right) \leq \eta_a, \tag{23}$$

where $\eta_s + \eta_a = \eta$. In particular, in this experiment, the risk level is equally split between the two single chance constraints, according to the naive risk level allocation $\eta_s = \eta_a = 0.025$.

Fig. 14 shows in purple lines the expected values of the optimal state variables, together with their 2-sigma confidence envelopes, obtained in the solution of this CCSOCP. The associated optimal control variables are represented in Fig. 15, and the corresponding vaccination and testing policies are shown in Fig. 16. For the sake of comparison, Figs. 14, 15, and 16 also show in green lines the optimal state and control variables, as well as the corresponding vaccination and testing strategies, obtained in the solution of the CCSOCP considered in Experiment 1.

The effect of the joint chance constraint (22) can be clearly seen in Fig. 14c and d, in which the 2-sigma confidence envelopes for the proportion of both symptomatic and asymptomatic subjects remain below the preset thresholds of 0.0006 and 0.006, respectively. Moreover, compared to the CCSOCP solved in Experiment 1, both confidence envelopes take lower values. These differences are mainly due to the increase in the testing and isolation of asymptomatic subjects during the first 50 days, as shown in Fig. 15b. Furthermore, in this case, it

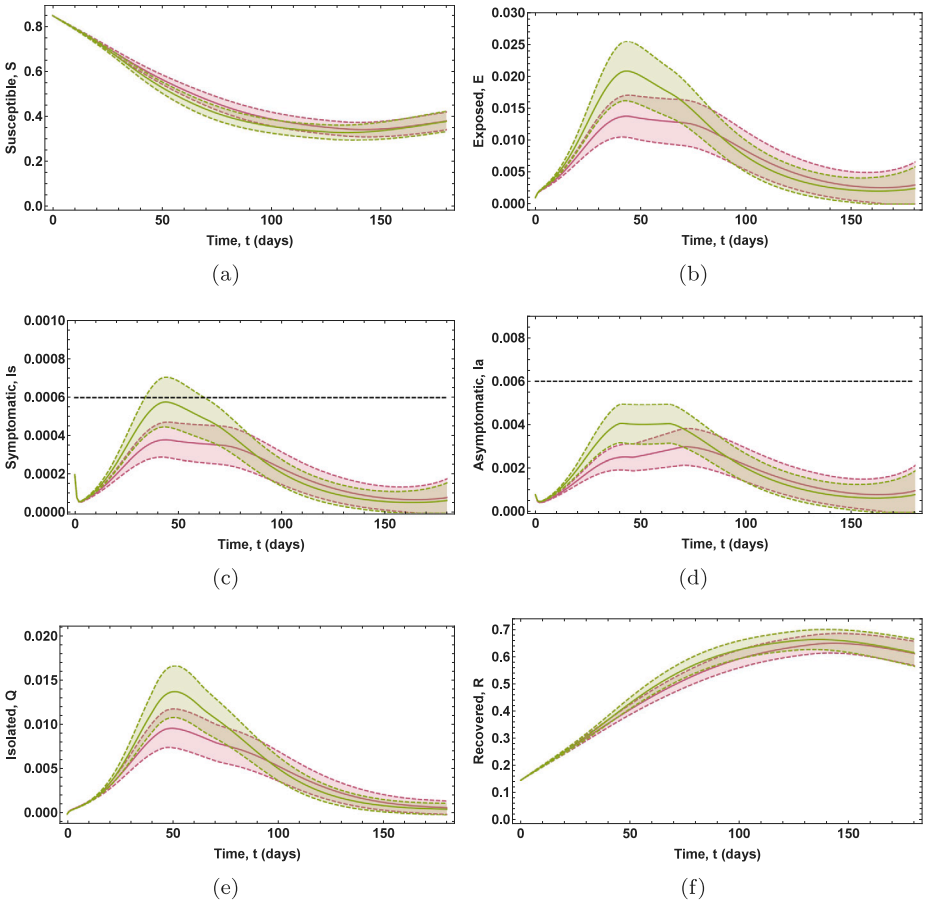

Fig. 14. Experiment 4. Expected values of the proportions of subjects in each compartment, together with their 2-sigma confidence envelopes. The curves corresponding to the solutions obtained with a single chance constraint and a joint chance constraint are shown in green and purple, respectively. The 2-sigma confidence envelopes for the proportion of both symptomatic and asymptomatic subjects represented in purple clearly remain below their corresponding preset thresholds due to the effect of the joint chance constraint (22). (For interpretation of the references to colour in this figure legend, the reader is referred to the web version of this article.)

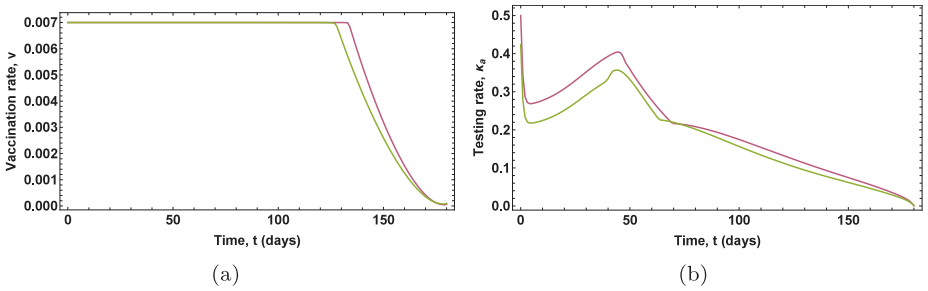

Fig. 15. Experiment 4. Optimal vaccination and testing rates. The curves corresponding to the solutions obtained with a single chance constraint and a joint chance constraint are shown in green and purple, respectively. There is a slight difference in the behaviour of the testing rate, whereas a more significant difference is observed in the testing and isolation of asymptomatic subjects during the first 50 days, in which the testing rate is higher when the joint chance constraint is considered. (For interpretation of the references to colour in this figure legend, the reader is referred to the web version of this article.)

can be concluded that the fulfilment of the chance constraint on the proportion of symptomatic subjects is the main responsible for the increase in the testing rate, which also implies a significant reduction in the proportion of asymptomatic, exposed, and isolated subjects, as can be seen in Fig. 14b, d, and e, respectively.

The surrogate models provided by the aPC expansion (9) not only allow for the estimation of the marginal PDFs of the optimal state variables at each time instant $t \in [t_i, t_F]$, but also the estimation of their joint PDFs, which enable a great variety of multivariate statistical analyses to be conducted. For instance, given two time instants t_1 and t_2, with $t_2 > t_1$, conditional probabilities of the form

$$P\left(I_s(t_2,\xi) \geq I_{s_U} \mid I_a(t_1,\xi) \geq I_{a_U}\right)$$

can be computed. Therefore, the threshold violation probability for the proportion of symptomatic subjects at time instant t_2 can be updated according to the proportion of asymptomatic subjects previously observed at a given time instant t_1.

In particular, the joint PDF and CDF of $I_s(t,\xi)$ and $I_a(t,\xi)$ at time instants $t = 70$ days and $t = 40$ days, respectively, have been estimated using a Gaussian kernel estimator, which are shown in Fig. 17, and the

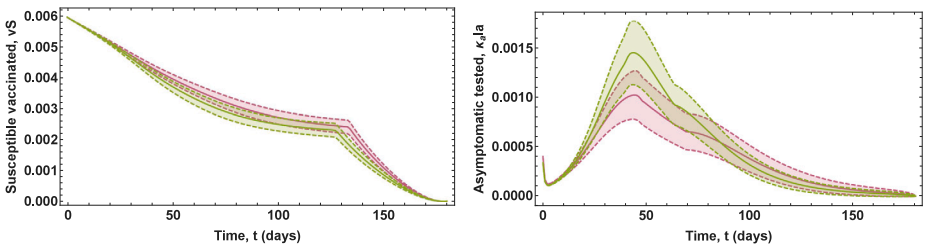

(a) (b)

Fig. 16. Experiment 4. Expected values of the proportion of susceptible vaccinated and asymptomatic tested subjects, together with their 2-sigma confidence envelopes. The curves corresponding to the solutions obtained with a single chance constraint and a joint chance constraint are shown in green and purple, respectively. The joint chance constraint (22) implies a slight increase in the vaccination policy and a decrease in the testing policy during the first 70 days. (For interpretation of the references to colour in this figure legend, the reader is referred to the web version of this article.)

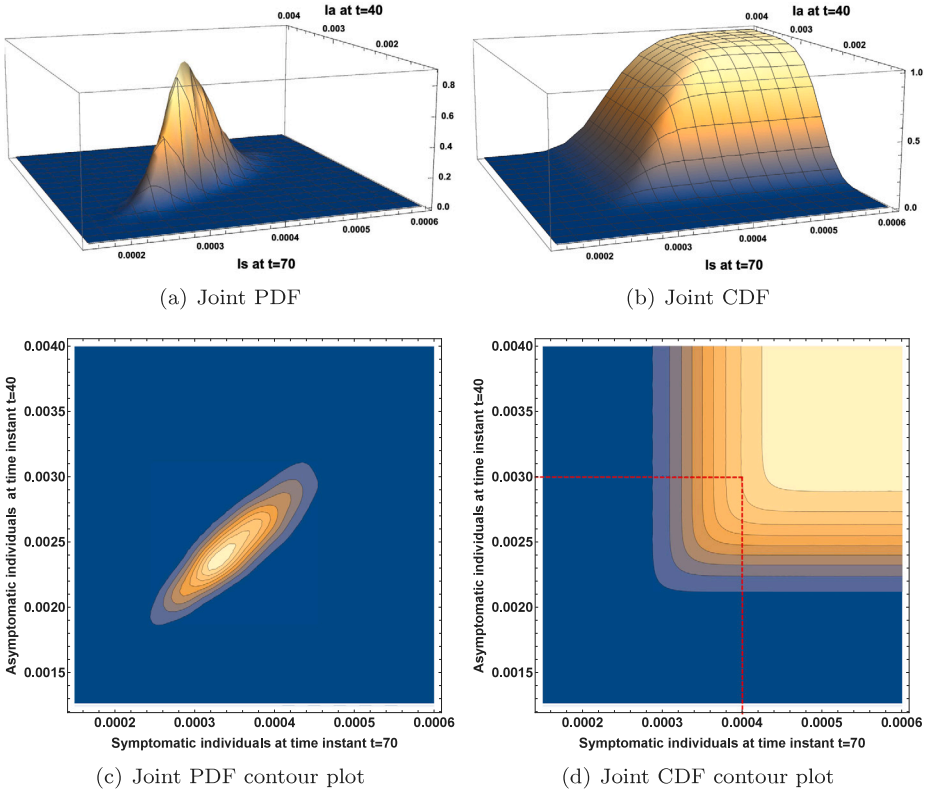

(a) Joint PDF (b) Joint CDF

(c) Joint PDF contour plot (d) Joint CDF contour plot

Fig. 17. Experiment 4. Joint PDF and CDF of variables I_s and I_a obtained in the solution of the CCSOCP at time instants $t = 40$ days and $t = 70$ days, respectively.

following conditional probability has been calculated:

$$P\left(I_s(70,\xi) \geq 0.0004 \mid I_a(40,\xi) \geq 0.003\right) = 0.9561.$$

Since $P\left(I_s(70,\xi) \geq 0.0004\right) = 0.1897$, it can be concluded that the threshold violation probability for the proportion of symptomatic subjects on day 70 will considerably increase if one month before the proportion of asymptomatic subjects exceeds 0.003.

Finally, Fig. 18 shows the Sobol' indices associated with all the optimal state variables obtained in the solution of the CCSOCP with both the single chance constraint and the joint chance constraint represented in dashed and solid lines, respectively. The corresponding Sobol' indices for the random parameters θ, ε, and δ are plotted in blue, orange, and green colours, respectively.

It can be seen that the variance of the proportion of exposed, symptomatic, asymptomatic, and isolated subjects, due to the variance of parameter ε is almost negligible, whereas the variance of the proportion of susceptible and recovered subjects reaches small but significant values during the first 30 days. Besides, the relative influence of the variance of the parameters θ and δ on the variance of the proportion of exposed, symptomatic, asymptomatic, and isolated subjects changes along the time period considered. Specifically, the variance of θ has the most influence on the variance of these state variables during the first 80 days, whereas the influence of the variance of δ becomes predominant the following 100 days. Moreover, no significant differences are observed between the Sobol' indices computed from the CCSOCP with the single chance constraint and the joint chance constraint, which show similar patterns along the whole time period considered.

9. Conclusions

In this paper, a spectral approach to the uncertainty management in epidemic models, based on the formulation of chance-constrained stochastic optimal control problems, has been presented, in which the inclusion of both single and joint chance constraints has been addressed. Moreover, a general procedure has been proposed to reformulate these chance-constrained stochastic optimal control problems as augmented deterministic optimal control problems, which can be solved using traditional numerical methods.

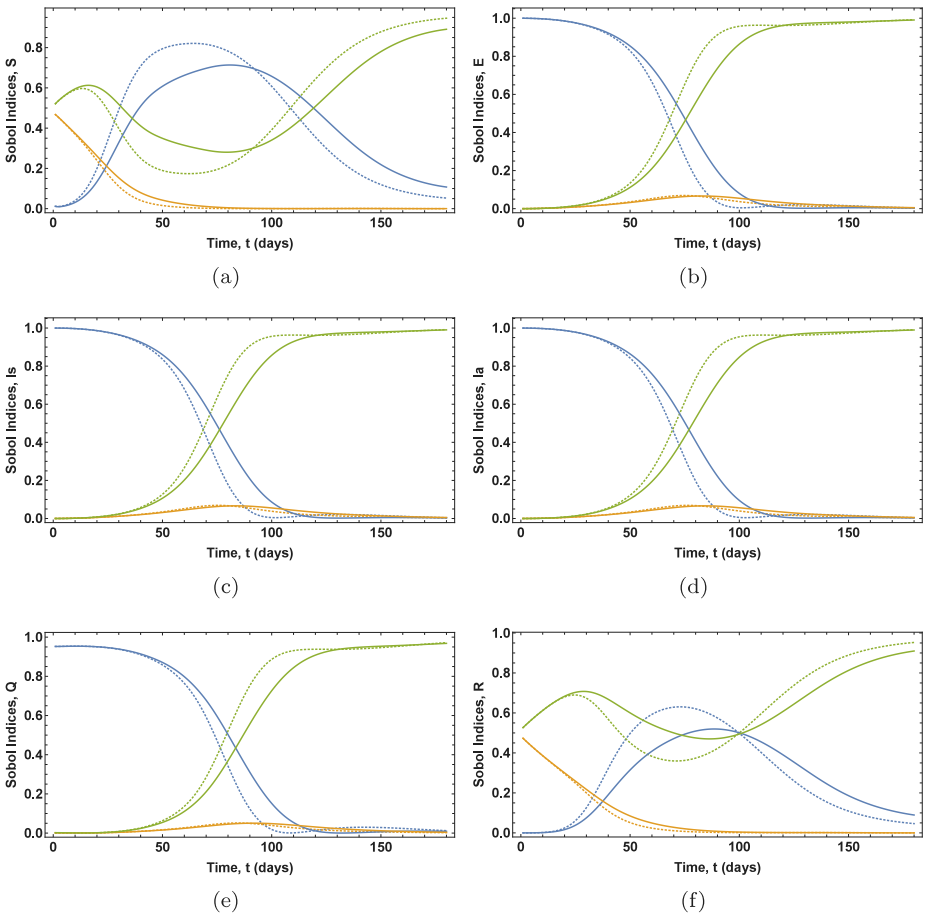

Fig. 18. Experiment 4. Sobol' indices for the random parameters θ (blue), ε (orange), and δ (green). The curves corresponding to the solutions obtained with a single chance constraint and a joint chance constraint are shown in dashed and solid lines, respectively. No significant differences are observed between the Sobol' indices computed from the CCSOCP with the single chance constraint and the joint chance constraint, which show similar patterns along the whole time period considered. (For interpretation of the references to colour in this figure legend, the reader is referred to the web version of this article.)

The arbitrary polynomial chaos expansion technique has been employed for the computation of surrogate models of the optimal stochastic state variables, whose main statistics can be efficiently computed. Then, applying the Chebyshev–Cantelli's inequality, the expected value and variance of these surrogate models have been used to reformulate single chance constraints. Moreover, joint chance constraints have been represented in terms of sets of single chance constraints by means of the Bonferroni's inequality. Furthermore, the surrogate models have also been employed to conduct a global sensitivity analysis in terms of the Sobol' indices, as well as a risk assessment analysis based on Monte Carlo simulations and kernel density estimations of the marginal and joint probability density functions of the optimal stochastic state variables at each time instant.

The practical application of the proposed methodology has been illustrated through several numerical experiments in which a COVID-19 epidemic model has been considered. Specifically, various stochastic optimal control problems have been solved, which include single and joint chance constraints as well as single and separate robust constraints. The effects of chance constraints and robust constraints on the solutions of the stochastic optimal control problems have been compared and discussed. The numerical results show that the inclusion of suitable chance constraints in the formulation of stochastic optimal control problems gives the designers of the optimal control strategies an efficient tool to quantify and manage the uncertainty in epidemic models. In addition, the proposed methodology, which is based on the use of chance constraints, provides the capability to increase the predictability of the outcomes in comparison with the results obtained when robust constraints are imposed.

Declaration of competing interest

The authors declare that they have no known competing financial interests or personal relationships that could have appeared to influence the work reported in this paper.

Data availability

No data was used for the research described in the article.

Acknowledgement

All authors have read and agreed to the published version of the manuscript.

References

[1] Maitre OL, Knio OM. Spectral methods for uncertainty quantification: With applications to computational fluid dynamics. Scientific computation, Springer; 2010.
[2] Brauer F, van den Driessche P, Wu J. Mathematical epidemiology. Springer; 2008.
[3] Brauer F, Castillo-Chavez C, Feng Z. Mathematical models in epidemiology. Springer; 2019.
[4] Han X, Kloeden PE. Random ordinary differential equations and their numerical solution. Probability theory and stochastic modelling, vol. 85, Springer; 2017.
[5] Ladde GS, Sambandham M. Stochastic versus deterministic systems of differential equations. CRC pure and applied mathematics, Chapman and Hall; 2003.
[6] Britton T, Pardoux E. Stochastic epidemic models with inference. Springer; 2019.

[7] Lototsky SV, Rozovsky BL. Stochastic partial differential equations. Springer; 2017.
[8] Ali HM, Ameen IG. Optimal control strategies of a fractional order model for Zika virus infection involving various transmissions. Chaos Solitons Fractals 2021;146:110864.
[9] Saha S, Samanta G. Analysis of a host-vector dynamics of a dengue disease model with optimal vector control strategy. Math Comput Simulation 2022;195:31–55.
[10] Rabiu M, Willie R, Parumasur N. Optimal control strategies and sensitivity analysis of an HIV/AIDS-Resistant model with behavior change. Acta Biotheor 2021;69:543–89.
[11] Barik M, Swarup C, Singh T, Habbi S, Chauhan S. Dynamical analysis, optimal control and spatial pattern in an influenza model with adaptive immunity in two stratified population. AIMS Math 2021;7(4):4898–935.
[12] Ali A, Iqbal Q, Asamoah JKK, Islam S. Mathematical modeling for the transmission potential of Zika virus with optimal control strategies. Eur Phys J Plus 2022;137:146.
[13] Srivastav AK, Srivastava AKPK, Ghosh M. Modeling and optimal control of dengue disease with screening and information. Eur Phys J Plus 2021;136:1187.
[14] Wattanasirikosone R, Modnak C. Analysing transmission dynamics of HIV/AIDS with optimal control strategy and its controlled state. J Biol Dyn 2022;16(1):499–527.
[15] Abbasi Z, Zamani I, Mehra AHA, Ibeas A, Shafieirad M. Optimal allocation of vaccine and antiviral drugs for influenza containment over delayed multiscale epidemic model considering time-dependent transmission rate. Comput Math Methods Med 2021;2021:4348910.
[16] Cui X, Xue D, Pan F. Dynamic analysis and optimal control for a fractional-order delayed SIR epidemic model with saturated treatment. Eur Phys J Plus 2022;137:586.
[17] Liu P, Din A, Huang L, Yusuf A. Stochastic optimal control analysis for the hepatitis B epidemic model. Results Phys 2021;26:104372.
[18] Azimi V, Sharifi M, Fakoorian S, Nguyen T, Huynh VV. State estimation-based robust optimal control of influenza epidemics in an interactive human society. Inform Sci 2022;592:340–60.
[19] Din A, Li Y. Stationary distribution extinction and optimal control for the stochastic hepatitis B epidemic model with partial immunity. Phys Scr 2021;96:074005.
[20] Chang K, Zhang Q, Yuan H. Stationary distribution and control strategy of a stochastic dengue model with spatial diffusion. J Appl Anal Comput 2022;12(1):153–78.
[21] Lv W, He H, Li K. Robust optimal control of a network-based SIVS epidemic model with time delay. Chaos Solitons Fractals 2022;161:112378.
[22] Din A, Li Y. Stochastic optimal analysis for the hepatitis B epidemic model with Markovian switching. Math Methods Appl Sci 2022;Early View.
[23] Hwang Y, Kwon H-D, Lee J. Optimal control problem of various epidemic models with uncertainty based on deep reinforcement learning. Numer Methods Partial Differential Equations 2022;Early View.
[24] Watkins NJ, Nowzari C, Pappas GJ. Robust economic model predictive control of continuous-time epidemic processes. IEEE Trans Automat Control 2019;65(3):1116–31.
[25] Péni T, Csutak B, Szederkényi G, Röst G. Nonlinear model predictive control with logic constraints for COVID-19 management. Nonlinear Dynam 2020;102:1965–86.
[26] Carli R, Cavone G, Epicoco N, Scarabaggio P, Dotoli M. Model predictive control to mitigate the COVID-19 outbreak in a multi-region scenario. Annu Rev Control 2020;50:373–93.
[27] Parino F, Zino L, Calafiore GC, Rizzo A. A model predictive control approach to optimally devise a two-dose vaccination rollout: A case study on COVID-19 in Italy. Internat J Robust Nonlinear Control 2021;Early View.
[28] Aldila D, Shahzad M, Khoshnaw SH, Ali M, Sultan F, Islamilova A, Anwar YR, Samiadji BM. Optimal control problem arising from COVID-19 transmission model with rapid-test. Results Phys 2022;37:105501.
[29] Khan AA, Ullaha S, Amin R. Optimal control analysis of COVID-19 vaccine epidemic model: a case study. Eur Phys J Plus 2022;137(1):156.
[30] Dhaibana AK, Jabbar BK. An optimal control model of the spread of the COVID-19 pandemic in Iraq: Deterministic and chance-constrained model. J Intell Fuzzy Syst 2021;40:4573–87.
[31] Scarabaggio P, Carli R, Cavone G, Epicoco N, Dotoli M. Nonpharmaceutical stochastic optimal control strategies to mitigate the COVID-19 spread. IEEE Trans Autom Sci Eng 2022;19(2):560–75.
[32] Li Y, Wei Z. Dynamics and optimal control of a stochastic coronavirus (COVID-19) epidemic model with diffusion. Nonlinear Dynam 2022;109:91–120.
[33] Wang R, Wang Q. Determination and estimation of optimal quarantine duration for infectious diseases with application to data analysis of COVID-19. Biometrics 2022;78(2):691–700.
[34] Armaou A, Katch B, Russo L, Siettos C. Designing social distancing policies for the COVID-19 pandemic: A probabilistic model predictive control approach. Math Biosci Eng 2022;19(9):8804–32.
[35] Thul L, Powell W. Stochastic optimization for vaccine and testing kit allocation for the COVID-19 pandemic. European J Oper Res 2023;304(3):325–38.
[36] Piprek P, Gros S, Holzapfel F. Rare event chance-constrained optimal control using polynomial chaos and subset simulation. Processes 2019;7(4):185.
[37] Keil RE, Miller AT, Kumar M, Rao AV. Method for solving chance constrained optimal control problems using biased kernel density estimators. Optim Control Appl Methods 2020;42(1):330–54.
[38] Gopalakrishnan B, Singh AK, Krishna KM, Manocha D. Solving chance-constrained optimization under nonparametric uncertainty through Hilbert space embedding. IEEE Trans Control Syst Technol 2021;30(2):901–16.
[39] Sun X, Zhang B, Chai R, Tsourdos A, Chai S. UAV trajectory optimization using chance-constrained second-order cone programming. Aerosp Sci Technol 2022;121:107283.
[40] Wiener N. The homogeneous chaos. Amer J Math 1938;60(4):897–936.
[41] Xiu D, Karniadakis GE. The Wiener–Askey Polynomial Chaos for stochastic differential equations. SIAM J Sci Comput 2002;24(2):619–44.
[42] Oladyshkin S, Nowak W. Data-driven uncertainty quantification using the arbitrary polynomial chaos expansion. Reliab Eng Syst Saf 2012;106:179–90.
[43] Hover FS, Triantafyllou MS. Application of polynomial chaos in stability and control. Automatica 2006;42:789–95.
[44] Kim K-KK, Braatz RD. Generalised polynomial chaos expansion approaches to approximate stochastic model predictive control. Internat J Control 2013;86(8):1324–37.
[45] Olivares A, Staffetti E. Optimal control-based vaccination and testing strategies for COVID-19. Comput Methods Programs Biomed 2021;211:106411.
[46] Zymler S, Kuhn D, Rustem B. Distributionally robust joint chance constraints with second-order moment information. Math Program 2013;137(1–2):167–98.
[47] Park GL, Lee TH, Lee KH, Hwang KH. Robust design: An overview. AIAA J 2006;44(1):181–91.
[48] Li X, Nair PB, Zhang Z, Gao L, Gao C. Aircraft robust trajectory optimization using nonintrusive polynomial chaos. J Aircr 2014;51(5):1592–603.
[49] Ahlfeld R, Belkouchi B, Montomoli F. SAMBA: Sparse approximation of moment-based arbitrary polynomial chaos. J Comput Phys 2016;320(529):1–16.
[50] Xiu D. Numerical methods for stochastic computations. A spectral method approach. Princeton University Press; 2010.
[51] Judd KL, Maliar L, Maliar S, Valero R. Smolyak method for solving dynamic economic models: Lagrange interpolation, anisotropic grid and adaptive domain. J Econom Dynam Control 2014;44:92–123.
[52] Gramacki A. Nonparametric kernel density estimation and its computational aspects. Springer; 2018.
[53] Trucchia A, Egorova V, Pagnini G, Rochoux M. On the merits of sparse surrogates for global sensitivity analysis of multi-scale nonlinear problems: Application to turbulence and fire-spotting model in wildland fire simulators. Commun Nonlinear Sci Numer Simul 2019;73:120–45.
[54] Olivares A, Staffetti E. Uncertainty quantification of a mathematical model of COVID-19 transmission dynamics with mass vaccination strategy. Chaos Solitons Fractals 2021;146:110895.
[55] Hajiagha SHR, Hashemi SS, Mahdiraji HA, Azaddel J. Multi-period data envelopment analysis based on Chebyshev inequality bounds. Expert Syst Appl 2015;42:7759–67.
[56] Calafiore G, El-Ghaoui L. On distributionally robust chance-constrained linear programs. J Optim Theory Appl 2006;130:1–22.
[57] Nakka YK, Liu A, Shi G, Anandkumar A, Yue Y, Chung S. Chance-constrained trajectory optimization for safe exploration and learning of nonlinear systems. IEEE Robot Autom Lett 2021;6(2):389–96.
[58] Herman AL, Conway BA. Direct optimization using collocation based on high-order Gauss-Lobatto quadrature rules. J Guid Control Dyn 1996;19(3):592–9.
[59] Manchein C, Brugnago EL, da Silva RM, Mendes CFO, Beims MW. Strong correlations between power-law growth of COVID-19 in four continents and the inefficiency of soft quarantine strategies. Chaos 2020;30:041102.
[60] Brugnago EL, da Silva RM, Manchein C, Beims MW. How relevant is the decision of containment measures against COVID-19 applied ahead of time? Chaos Solitons Fractals 2020;140:110164.
[61] Naaber P, Tserel L, Kangro K, Sepp E, Jürjenson V, Adamson A, Haljasmägi L, Rumm AP, Maruste R, Kärner J, Gerhold JM, Planken A, Ustav M, Kisand K, Peterson P. Dynamics of antibody response to BNT162b2 vaccine after six months: a longitudinal prospective study. Lancet Reg Health - Eur 2021;10:100208.
[62] Thomas SJ, Moreira ED, Kitchin N, Absalon J, Gurtman A, Lockhart S, Perez JL, Pérez Marc G, Polack FP, Zerbini C, Bailey R, Swanson KA, Xu X, Roychoudhury S, Koury K, Bouguermouh S, Kalina WV, Cooper D, Frenck RW, Hammitt LL, Türeci Ö, Nell H, Schaefer A, Ünal S, Yang Q, Liberator P, Tresnan DB, Mather S, Dormitzer PR, Şahin U, Gruber WC, Jansen KU. Safety and efficacy of the BNT162b2 mRNA COVID-19 vaccine through 6 months. N Engl J Med 2021;385:1761–73.
[63] Olivares A, Staffetti E. Optimal control applied to vaccination and testing policies for COVID-19. Mathematics 2021;9:3100.
[64] US Food and Drug Administration. Pfizer-Biontech COVID-19 Vaccine. Briefing Document. 2020, URL.
[65] Li Q, et al. Early transmission dynamics in Wuhan, China, of novel coronavirus–infected pneumonia. 382, 2020, p. 1199–207,
[66] Wu JT, Leung K, Leung GM. Nowcasting and forecasting the potential domestic and international spread of the 2019-nCoV outbreak originating in Wuhan, China: A modelling study. Lancet 2020;395:689–97.
[67] European Medicines Agency. COVID-19: latest updates. 2020, URL.
[68] UK Medicines and Healthcare Products Regulatory Agency. Information for Healthcare Professionals on Pfizer/BioNTech COVID-19 vaccine. 2020, URL.